

# Testing and Improving the Robustness of Amortized Bayesian Inference for Cognitive Models

Yufei Wu<sup>1,\*</sup>, Stefan T. Radev<sup>2</sup>, and Francis Tuerlinckx<sup>1</sup>

<sup>1</sup>University of Leuven, Belgium

<sup>2</sup>Rensselaer Polytechnic Institute, US

\*Corresponding author: [yufei.wu@kuleuven.be](mailto:yufei.wu@kuleuven.be)

## Abstract

Contaminant observations and outliers often cause problems when estimating the parameters of cognitive models, which are statistical models representing cognitive processes. In this study, we test and improve the robustness of parameter estimation using amortized Bayesian inference (ABI) with neural networks. To this end, we conduct systematic analyses on a toy example and analyze both synthetic and real data using a popular cognitive model, the Drift Diffusion Models (DDM). First, we study the sensitivity of ABI to contaminants with tools from robust statistics: the empirical influence function and the breakdown point. Next, we propose a data augmentation or noise injection approach that incorporates a contamination distribution into the data-generating process during training. We examine several candidate distributions and evaluate their performance and cost in terms of accuracy and efficiency loss relative to a standard estimator. Introducing contaminants from a Cauchy distribution during training considerably increases the robustness of the neural density estimator as measured by bounded influence functions and a much higher breakdown point. Overall, the proposed method is straightforward and practical to implement and has a broad applicability in fields where outlier detection or removal is challenging.

**Keywords:** robust estimation, Amortized Bayesian Inference, Drift Diffusion Model, outliers, Cauchy Distribution, deep neural networks

## Introduction

Identifying and appropriately handling outliers is both unavoidable and essential for drawing accurate conclusions from quantitative data. Outliers are observations that deviate significantly from the majority of data points (Aggarwal, 2017; Hawkins, 1980) and are

often generated by processes different from the process under study. For example, in behavioral science, careless responding is a major source of outliers (Maniaci & Rogge, 2014). Commencing with Huber’s foundational work (1964) on M-estimators for estimating the mean of a univariate normal distribution, the field of robust statistics has generated a number of methods for detecting and dealing with outliers (Donoho & Huber, 1982; Hawkins, 1980; Tukey, 1979; Hampel et al., 2005). If not properly addressed, outliers may have unduly large effects on the parameter estimates of statistical models and ultimately lead to wrong conclusions.

However, not all outliers are contaminants. Some outliers may also be generated by the process under study, in which case the extreme observation is the result of mere chance. Similarly, not every contaminant is an outlier. An observation not generated by the process under study may result in a numerical value that is difficult or even impossible to distinguish from the majority of observations (and is unobtrusive when the proportion of contaminants is low). In this study, we examine contaminants that may appear either as outliers or blend with most of the observations. Unless specifically emphasized, we use “contaminant” and “outlier” interchangeably.

Among the various statistical and computational models in psychology, some are particularly vulnerable to outliers due to the nature of their underlying assumptions. For example, the widely used Drift Diffusion Model (DDM; Ratcliff, 1978), which is used to explain patterns in choice reaction time data from perceptual decision-making tasks, includes parameters that characterize the underlying decision-making process. In the most basic variant of the DDM, a key parameter is the non-decision time ( $T_{er}$ ), which represents the time taken for stimulus encoding and motor execution. By design,  $T_{er}$  is estimated to be lower than the shortest reaction time in the data set. Since the decision process is jointly determined by all DDM parameters, when a short outlier is present, it can distort not only the estimate of  $T_{er}$  but also those of other parameters, leading to biased results. Consequently, addressing the influence of outliers has been a persistent challenge in DDM fitting (Ratcliff, 1993; Ratcliff & Rouder, 1998; Ratcliff & Tuerlinckx, 2002; Myers et al., 2022).

The simplest approach to managing outliers is to apply hard cutoffs or bounds to the raw data, such as Tukey’s fences (Tukey, 1977). However, this approach is only effective for clearly distinguishable outliers and fails to address more subtle contaminants. Thus, various more sophisticated methods have been proposed to reduce the impact of outliers in model fitting (Maronna et al., 2006; Sumarni et al., 2017; Aggarwal, 2017). When model fitting is based on maximum likelihood estimation (MLE) or Bayesian approaches using Markov chain Monte Carlo (MCMC) sampling (Kruschke, 2011), robust methods often require modifying the loss or the likelihood function of the model. This introduces two key challenges. First, modifying the loss function can be impractical for many model users. Second, not all models have an explicitly available loss function or likelihood, which limits the range of feasible actions.

In this paper, we do not work in a traditional statistical framework to estimate model parameters. Instead, we opt for a simulation-based approach combined with deep neural networks. More specifically, we use amortized Bayesian inference (ABI, Zammit-Mangion et al., 2024), which is a particular case of simulation-based inference (Cranmer et al., 2020). ABI leverages model simulations as training data for powerful deep neural networks that are optimized to encode structural and functional knowledge about the simulation model and its parameters. By recasting the costly posterior sampling task as forward passes through a pre-trained neural network, these methods can achieve nearly instantaneous (i.e., *amortized*) parameter inference for new data sets (Gonçalves et al., 2020; Radev et al., 2020). Throughout this paper, we refer to these neural networks as the neural density estimator. Crucially, these methods bypass the evaluation of the likelihood (hence their alternative designation as “likelihood-free”) and avoid expensive MCMC sampling or likelihood approximations altogether, making them an attractive and versatile addition to the modeler’s toolkit (Schmitt et al., 2024a).

However, amortized methods have been shown to be more susceptible to estimation errors than their non-amortized counterparts (e.g., MCMC) in the presence of *model misspecification* (Schmitt et al., 2021). Thus, previous work has focused on inducing *robust* amortized estimators (Ward et al., 2022; Huang et al., 2024; Siahkoohi et al., 2023; Kelly et al., 2024), but these methods either require non-trivial modifications to the straightforward simulation-based training or sacrifice the amortization property. Since contaminants can be viewed as a special case of model misspecification (Schmitt et al., 2021), they present a serious obstacle for the adoption of amortized methods across behavioral and the cognitive sciences, where computational models are nearly always approximations and data tends to be noisy, unpredictable, and corrupted in unexpected ways.

In this study, we investigate the influence of outliers using tools from robust statistics and propose a simple data augmentation approach to enhance the robustness of ABI in cognitive modeling. To clarify the use of amortized Bayesian inference, we compare amortized and traditional inference methods and conduct a systematic empirical investigation into the meaning of learnable summary statistics. The univariate normal distribution and DDM serve as test beds to demonstrate our robust methodology. Our approach can be extended to a wide range of other stochastic models of cognition, whether likelihood-based or simulation-based.

## Amortized Bayesian Inference

Amortized methods utilize model simulations to train specialized neural networks that learn to compress data of varying sizes and sample from the posterior of model parameters given *any* data set compatible with the model (Zammit-Mangion et al., 2024).

A simple amortized workflow is depicted in Figure 1. During the training phase, the initial step involves defining a wide prior  $\boldsymbol{\theta} \sim p(\boldsymbol{\theta})$  and a generative model  $\boldsymbol{x} \sim p(\boldsymbol{x} | \boldsymbol{\theta})$ ,

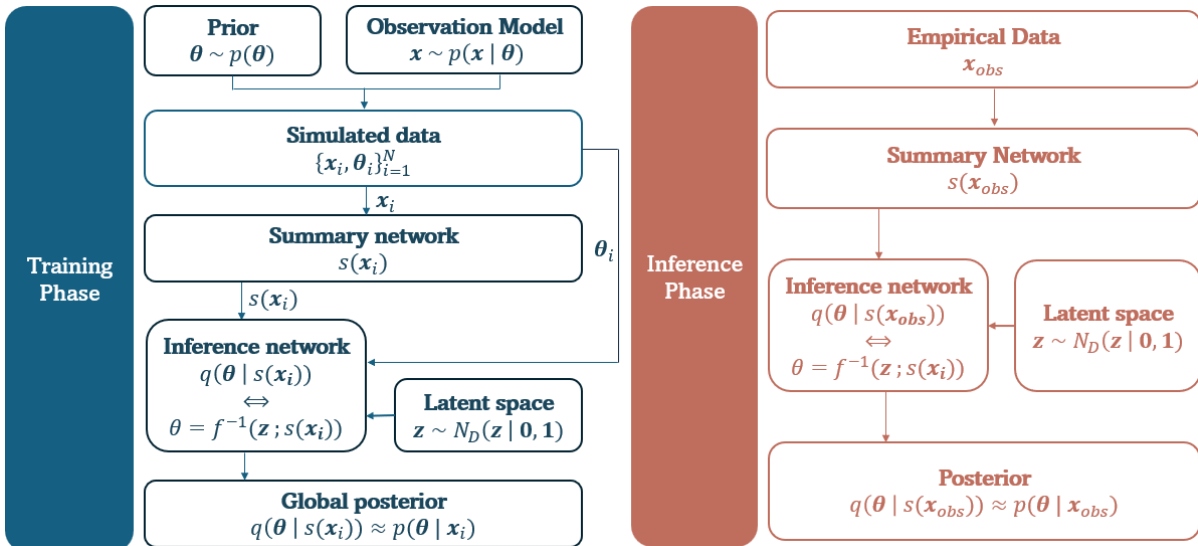


Figure 1: The basic workflow of amortized Bayesian inference (ABI) for posterior estimation. Parameters and data are simulated from a prior and an observation model. The simulations are used as training data for the summary and inference networks that jointly learn a global posterior. Once the networks are trained, they can instantly sample from the approximate posterior conditioned on any actually observed data.

where  $\boldsymbol{\theta} \in \mathbb{R}^D$ . Subsequently, parameters are simulated from the prior and passed to the generative model to generate synthetic data sets. The simulated parameters and data sets  $\{\boldsymbol{x}_i, \boldsymbol{\theta}_i\}_{i=1}^I$  are used to train two neural networks: a summary and an inference network. The summary network transforms each data set  $\boldsymbol{x}_i$  into fixed-size *approximately sufficient* summary statistics  $s(\boldsymbol{x}_i)$ , where  $s(\cdot)$  represents the transformation applied by the summary network. Meanwhile, the inference network learns to approximate the true posterior of model parameters given  $\boldsymbol{x}$  as accurately as possible:

$$q(\boldsymbol{\theta} | s(\boldsymbol{x})) \approx p(\boldsymbol{\theta} | \boldsymbol{x}), \quad (1)$$

Approximating complex posterior distributions involves sampling from high-dimensional conditional probability distributions, which is a non-trivial computational task. However, recent advancements in generative deep learning provide a wide range of expressive algorithms to address this challenge (e.g., Kobyzev et al., 2020; Lipman et al., 2022; Yang et al., 2023). For instance, normalizing flows (Kobyzev et al., 2020) learn an invertible transformation  $f$  between the complex target distribution and a predefined simple latent distribution  $\boldsymbol{z}$  (e.g., a spherical Gaussian), such that sampling from  $\boldsymbol{z}$  and applying the inverse  $f^{-1}$  yields samples from the approximate posterior:

$$\boldsymbol{\theta} \sim q(\boldsymbol{\theta} | s(\boldsymbol{x})) \iff \boldsymbol{\theta} = f^{-1}(\boldsymbol{z}; s(\boldsymbol{x})) \text{ with } \boldsymbol{z} \sim \mathcal{N}_D(\boldsymbol{z} | \mathbf{0}, \mathbf{I}), \quad (2)$$

where  $f$  is an invertible function parameterized by a conditional invertible network (Arizzone et al., 2019; Radev et al., 2020). The summary and inference networks are jointly optimized to ensure that the approximate posterior corresponds as closely as possible to

the true posterior. The parameters of the neural networks are learned by minimizing the Kullback-Leibler (KL) divergence between the true and the approximate posterior for any data set  $\mathbf{x}$  sampled from the prior predictive distribution  $p(\mathbf{x})$  (for more details, please refer to Kullback & Leibler, 1951; Radev et al., 2020):

$$(f^*, t^*) = \operatorname{argmin}_{f, t} \mathbb{E}_{p(\mathbf{x})} \left[ \mathbb{KL}(p(\boldsymbol{\theta} | \mathbf{x}) || q(\boldsymbol{\theta} | s(\mathbf{x}))) \right]. \quad (3)$$

Upon convergence, the neural networks acquire an approximate representation of the full posterior. In practice, we define a prior distribution broad enough to generate a realistic range of empirical data. The inference phase (see Figure 1) is then straightforward: the observed data  $\mathbf{x}^{(obs)}$  is fed into the networks, and the corresponding posterior can be inferred without any overhead.

More recent amortized algorithms employ multi-step continuous-time models, such as flow-matching (Dax et al., 2023), diffusion models (Simons et al., 2023), and few-step consistency models (Schmitt et al., 2024b). In this study, we focus on normalizing flows, the simplest family of deep probabilistic models that works sufficiently well in practice.

## Drift Diffusion Model

The Drift Diffusion Model (DDM) is by far the most popular cognitive model for fitting choice reaction time data in terms of neurocognitively plausible parameters (Ratcliff, 1978; Ratcliff et al., 2016; Usher & McClelland, 2001). In choice reaction tasks, participants are typically asked to make binary decisions, such as determining the moving direction of a collection of largely random dots (left or right) (Mulder et al., 2012), classifying words and non-words (Ratcliff et al., 2004), or identifying old versus new items in memory tasks (Spaniol et al., 2006). Performance is then compared across different conditions (e.g., primed vs. non-primed words) or participant demographics (e.g., younger vs. older adults).

The DDM assumes that decision-making is a noisy evidence accumulation process, where in each trial the participant accumulates information until it reaches a decision boundary. This idea can be intuitively and graphically illustrated in Figure 2. The distance between the two boundaries is denoted as  $a$ , known as the boundary separation. The participant starts accumulating evidence from a point in between, denoted as the relative starting point or response bias  $z \in [0, 1]$ : If  $z > 0.5$  ( $z < 0.5$ ) then there is a bias towards the upper (lower) boundary, while if  $z = 0.5$ , there is no bias. The drift rate  $v$  represents the average rate of evidence accumulation under a specific condition. If there are two conditions, the drift rates are denoted as  $v_1$  and  $v_2$ . Finally, the non-decision time  $T_{er}$  accounts for any time unrelated to the decision process itself. These parameters in the standard DDM determine the distribution of reaction time and choice probabilities in decision-making tasks.

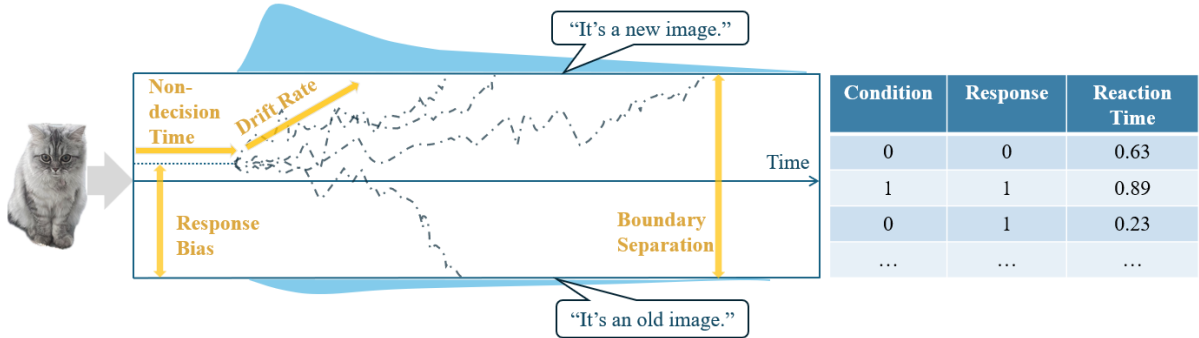


Figure 2: A graphical illustration of the drift diffusion process and the resulting reaction time data in a hypothetical visual recognition memory task. Participants view an image and judge whether it is old (i.e., previously seen) or new (i.e., previously unseen). The rows in the resulting data table correspond to individual trials of the experiment, with conditions and responses coded as 0 (old image) and 1 (new image).

Several variants of the basic DDM have been proposed (see e.g., Ratcliff & Tuerlinckx, 2002; Ratcliff & Rouder, 1998; Ratcliff et al., 2016; Wieschen et al., 2020), and in most of these variants trial-to-trial variability parameters have been added to non-decision time, drift rates and/or starting point. For reasons of simplicity, we focus on the standard version of the DDM in this paper. The reasons for this choice are twofold. First, the trial-to-trial variability parameters of the DDM often cause estimation problems (see e.g., Lerche & Voss, 2016; Tillman et al., 2020). Second, the basic variant of the DDM is an interesting case by itself to study robustness given the strong dependence of the non-decision time  $T_{er}$  on the minimum response time (as explained above).

Various methods exist for fitting the standard DDM: parameter estimation based on binning and minimizing a  $\chi^2$  loss function (Ratcliff & Tuerlinckx, 2002), maximum likelihood estimation (Ratcliff & Tuerlinckx, 2002), closed-form estimator for a simplified version (i.e., EZ diffusion, Wagenmakers et al., 2007), minimizing a Kolmogorov-Smirnov based loss function (Voss & Voss, 2008), and Markov Chain Monte Carlo (MCMC) methods to sample from the posterior distribution (Ahn et al., 2017). All these methods rely on the fact that, for the standard DDM version considered in this paper, the probability density function is known and has an analytical expression, which can be efficiently approximated via numerical integration. However, for many extensions of DDM, there is no explicit analytical expression for the likelihood. One such example is a model where the accumulation process is not Gaussian but is derived from a heavy-tailed distribution (Wieschen et al., 2020). In such a case, ABI offers a practical solution.

In this paper, we work with the standard DDM and estimate its parameters with ABI. Other methods exist for this model, but ABI allows for an efficient study of the impact of outliers on the model’s parameters. Although the DDM is known to be sensitive to outliers, few studies have directly explored their impact in DDM estimation. Different fitting methods (maximum likelihood estimation,  $\chi^2$ -square estimation, and weighted least

squares estimation, Kolmogorov-Smirnov method) are compared in the presence of contaminants, but their main focus was on comparing methods rather than an in-depth study of the precise impact of contaminants (Ratcliff & Tuerlinckx, 2002; Lerche et al., 2017). One reason for this gap is that large-scale simulation studies can be highly time-consuming with existing methods. However, recent progress in ABI (e.g., Von Krause et al., 2022) has made principled Bayesian workflows (Schad et al., 2021) extremely efficient. Thus, this study aims to systematically study the impact of outliers on DDM estimates under this framework. On the other hand, the analytical tractability of the standard DDM enables us to better understand the mechanisms underlying learned summary statistics in ABI, effectively unpacking the black box of the learning process.

Not only is the influence of outliers in DDM fitting understudied, but there is also no universal solution to the problem. A common approach involves setting absolute cutoffs for reaction times that are either too short or too long, and discarding trials that fall outside these predetermined limits (Myers et al., 2022). Common thresholds are RTs shorter than 100ms or 200ms or RTs longer than 2.5s or 3s. Alternative methods to mitigate the impact of outliers include transforming the data to normalize it or using cutoffs based on standard deviation or interquartile range. For example, one could take the log or inverse transformation of reaction time data and replace the observation that is 2 standard deviations above or below the mean by the observation *at* the 2 standard deviations above or below the mean (Ratcliff, 1993). While these methods might seem less arbitrary, they can significantly reduce statistical power and introduce their own biases (Ratcliff, 1993; Ulrich & Miller, 1994). More challenges arise when contaminants overlap with the distributions of genuine response times, making their identification and removal even more difficult (Ratcliff, 1993).

Overall, robustifying DDM estimation is challenging due to the model’s complexity within the conventional fitting framework, where directly modifying the loss function or likelihood is difficult. However, robust DDM estimation is crucial because the model’s assumptions make it particularly sensitive to outliers. This sensitivity makes the DDM an ideal test bed for evaluating our data augmentation approach within the framework of amortized Bayesian inference.

Before studying the impact of outliers and how we can diminish their influence, we will first study the performance and the mechanics of the ABI estimator on uncontaminated data and compare this to traditional estimators (such as MCMC-based Bayesian estimation).

## Parameter Recovery Study for the Drift Diffusion Model

To demonstrate the validity of our approach, we present a comparative study among ABI with the Python package *BayesFlow* (Radev et al., 2023), MCMC sampling using the R software JAGS and *dwiener* module (Wabersich & Vandekerckhove, 2014), and EZ

diffusion (Wagenmakers et al., 2007), to offer insights into the performance and inner workings of end-to-end amortized inference. JAGS was chosen because MCMC sampling remains the gold standard for fully Bayesian estimation of stochastic models, providing an external reference to evaluate ABI’s performance. EZ diffusion provides an analytic solution to estimating the key DDM parameters by fixing  $z = 0.5$ . Crucially, it relies on three *sufficient summary statistics*: the mean reaction time of correct responses ( $M_{RT}$ ), the variance of reaction time for correct responses ( $V_{RT}$ ), and the proportion of correct response ( $P_c$ ). The equations for the three sufficient summary statistics used in EZ diffusion are as follows:

$$P_c = \frac{1}{1 + \exp(h)} \quad (4)$$

$$M_{RT} = \left(\frac{a}{2v}\right) \frac{1 - \exp(h)}{1 + \exp(h)} + T_{er} \quad (5)$$

$$V_{RT} = \left(\frac{as^2}{2v^3}\right) \frac{2h \exp(h) - \exp(2h) + 1}{[\exp(h) + 1]^2}, \quad (6)$$

where  $h = \frac{-va}{s^2}$  and  $v \neq 0$ . The values of  $v$ ,  $a$ , and  $T_{er}$  can be derived by solving these three equations (Wagenmakers et al., 2007). Next, we estimate the DDM parameters with BayesFlow, JAGS, and the EZ-diffusion to investigate (1) the validity of our amortized Bayesian setup for recovering the parameters compared to simpler alternatives; and (2) the relationship between the summary statistics learned by the summary network and the simple statistics used by EZ-diffusion.

To perform ABI, we train neural networks with data simulated from a minimal DDM with  $z = 0.5$  and a single drift rate. Ground-truth parameter triplets  $(v, a, T_{er})$  are sampled from their corresponding prior distributions (refer to Table 1), with the within-trial noise variance  $s^2$  in the diffusion process fixed at 1. We choose a narrower joint prior compared to the typical practice in ABI, to align the typical set of parameters with the more conservative parameter range suitable for EZ diffusion, rather than cover the full spectrum of possible data sets (for an example, see Table 2). Subsequently, the parameters are fed into a generative model to generate choice reaction time data consisting of 200 trials. Every observation  $i$  (with  $i = 1, \dots, 200$ ) consists of a pair of a reaction time  $rt_i$  and choice  $y_i$ , jointly simulated from the Wiener process with a drift rate  $v$ , boundary separation  $a$ , starting point  $z = 0.5$ , and non-decision time  $T_{er}$ :

$$(rt_i, y_i) \sim \text{Wiener}(v, a, z = 0.5, T_{er}), \quad (7)$$

The reaction time data are log transformed as this was found to improve convergence.

The second step is to specify the ABI network architecture, which is guided by the model and data. As the DDM assumes independent and identically distributed (i.i.d.) trials, the order of observations (pairs of reaction times  $rt$  and choices  $y$ ) is irrelevant for the parameter estimation. Accordingly, we employ a permutation-invariant Set Trans-



former architecture (Lee et al., 2019) as a summary network and set the output dimension to three to align with the number of sufficient summary statistics calculated by the EZ diffusion method. For the inference network, we use a neural spline flow (Durkan et al., 2019) with six coupling layers. Training of the networks takes place over 100 epochs, with 1000 iterations per epoch and a batch size of 32. For all following training, we use the Adam optimizer with a starter learning rate of  $5 \times 10^{-4}$  and an exponential decay rate of .95.

Parameters	Distribution
$v$ (Drift rate)	$U(0.2, 2)$
$a$ (Boundary separation)	$U(0.5, 5)$
$T_{er}$ (Non-decision time)	$\text{Gamma}(1.5, 0.2)$

Table 1: Prior distributions for the comparison between BayesFlow, JAGS, and EZ diffusion.  $\text{Gamma}(1.5, 0.2)$  denotes a gamma distribution with shape parameter 1.5 and scale parameter 0.2. The range of the prior is relatively narrow to accommodate the conservative effective range in EZ diffusion.

After training, we simulate 500 new data sets to assess parameter recovery. For BayesFlow, we simply input the simulated data to the trained summary and inference networks and obtain the posterior samples. For JAGS, we specify four chains, with 1000 steps of adaptation, 1000 steps of burn-in, and 1000 samples per chain. The convergence of the MCMC chains is assessed by  $\hat{R}$  statistics (Gelman & Rubin, 1992), with a threshold of  $\hat{R} < 1.1$  indicating reasonable convergence. For the EZ diffusion, the parameters are calculated based on the Equations 4, 5, and 6. Out of 500 simulated data sets, 491 converge in JAGS, with non-convergent data sets discarded from estimations in all three methods to ensure comparability across all methods. There are no convergence issues with the other two methods.

As shown in Figure 3, except for the  $T_{er}$  estimated in EZ diffusion which sometimes take unrealistic negative values, most of the parameters are accurately recovered. Summary performance indices are reported in Table 2: the root mean squared error (RMSE) and the posterior standard deviation (of the marginal posterior for each parameter). The RMSE is defined as:  $RMSE_{\theta} = \sqrt{\frac{1}{n} \sum (\hat{\theta}_i - \theta_i)^2}$ . Regarding the RMSE, JAGS performs better than EZ diffusion in recovering non-decision time, but not for drift rate and boundary separation. However, BayesFlow outperforms JAGS and EZ diffusion in estimating all three parameters.

Regarding the posterior standard deviations, we only compared JASG to BayesFlow as EZ diffusion does not provide uncertainty quantifications. As shown in Table 2, with JAGS exhibiting lower uncertainty than BayesFlow for drift rate and boundary separation but higher errors. Overall, while EZ diffusion and JAGS perform well, BayesFlow excels in both accuracy and precision.

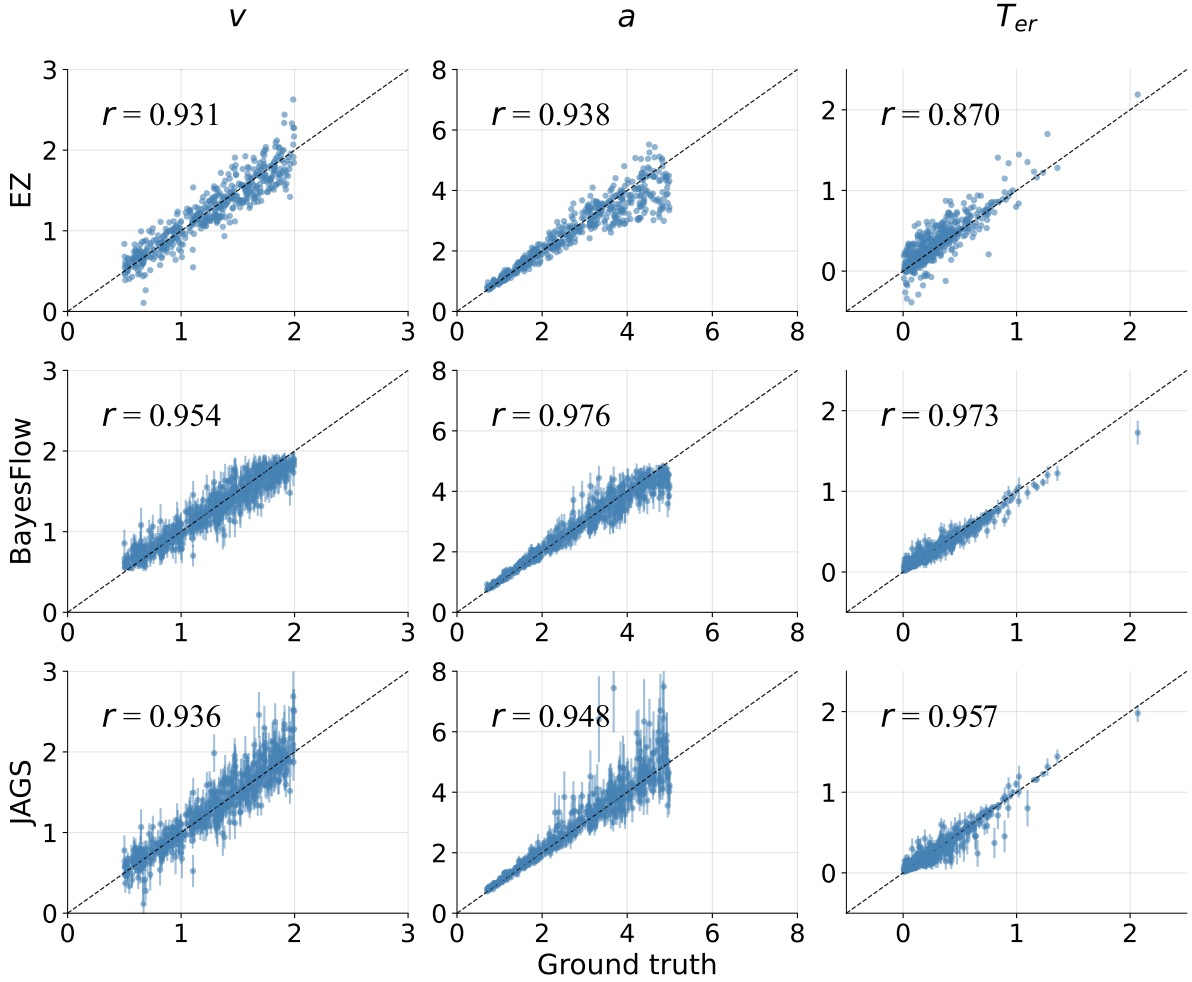


Figure 3: Parameter recovery of the minimal DDM with different estimators. The x- and y-axis show the ground truth and estimated values, respectively. The diagonal dashed lines indicate perfect recovery. In each subplot, the Pearson's correlation coefficient  $r$  quantifies the alignment between the estimated and true values. The error bars for JAGS and BayesFlow quantify the uncertainty by showing  $\pm$  posterior standard deviation around the point estimates.

	<i>RMSE</i>			posterior <i>SD</i>		
	EZ	BayesFlow	JAGS	EZ	BayesFlow	JAGS
$v$	0.161	0.132	0.173	/	0.149	0.128
$a$	1.923	0.283	0.457	/	0.307	0.240
$T_{er}$	1.025	0.063	0.073	/	0.055	0.050

Table 2: Performance comparison between methods based on *RMSE* and posterior *SD*. The *RMSE* and the posterior *SD* are calculated from estimates of 500 data sets using three distinct methods. Since EZ diffusion only provides point estimates, no standard deviation is available for this method, indicated by a slash (“/”).

## Interpreting the Learned Summary Statistics

Next, we investigate what the summary network in BayesFlow has learned during training. Given the high degree of agreement between estimation in EZ-diffusion and BayesFlow, it is reasonable to assume that the three learned summary statistics  $\mathbf{S}_B$  should contain the same information as the summary statistics for EZ diffusion, denoted as  $\mathbf{S}_{EZ} = (P_c, M_{RT}, V_{RT})$ . However, the mapping between  $\mathbf{S}_B$  and  $\mathbf{S}_{EZ}$  can be highly non-linear (see Figure A1 in Appendix).

To explore the relationship between  $\mathbf{S}_B$  and  $\mathbf{S}_{EZ}$ , we retrieve  $\mathbf{S}_B$  and  $\mathbf{S}_{EZ}$  for the 500 data sets that are used above, and build a multivariate random forest in the R package `MultivariateRandomForest` (Segal & Xiao, 2011). The multivariate random forest is a machine learning algorithm that can capture complex, non-linear relationship and make prediction in a non-parametric manner (Segal & Xiao, 2011). We train a multivariate random forest with 250 sets of data pair  $(\mathbf{S}_B, \mathbf{S}_{EZ})$  and use the remaining 250  $\mathbf{S}_B$  as a test set to predict the corresponding  $\mathbf{S}_{EZ}$ .

As shown in Figure 4, the correlation coefficient between the true  $\mathbf{S}_{EZ}$  and  $\hat{\mathbf{S}}_{EZ}$  predicted by  $\mathbf{S}_{BF}$  is higher than 0.9. This empirical result is not surprising (Radev et al., 2020), yet it convincingly demonstrates that summary networks learn a representation of the data that is in line with the information used by analytical methods.

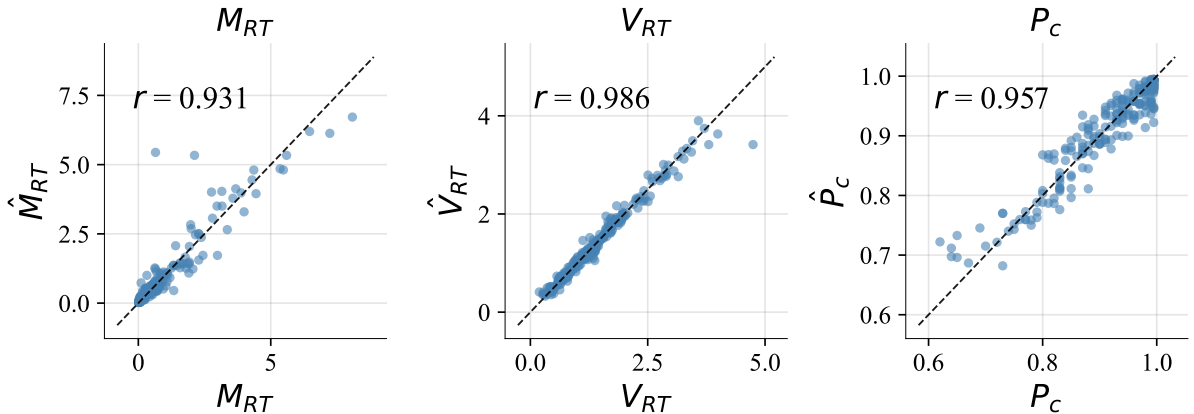


Figure 4: Predicted sufficient summary statistics  $\hat{\mathbf{S}}_{EZ}$  from  $\mathbf{S}_B$ . As the figure shows, the y-axis is the  $\hat{M}_{RT}$ ,  $\hat{V}_{RT}$  and  $\hat{P}_c$  predicted by  $\mathbf{S}_B$ , and the x-axis are the observed values of  $M_{RT}$ ,  $V_{RT}$ , and  $P_c$ .

In summary, we have demonstrated how BayesFlow can be used to fit a diffusion model and we have assessed its performance. Additionally, we have examined the information represented by the summary network by comparing the learned summary statistics in BayesFlow with the summary statistics used in the EZ diffusion method. This shows that the summary network is capable of learning an *approximately sufficient* summary of the data set.

## The Impact of Outliers in Amortized Bayesian Inference

In this section, we will introduce two tools from robust statistics (Maronna et al., 2006) to assess the robustness of neural density estimators to outliers. Specifically, we will use the empirical influence function (EIF; Cook & Weisberg, 1980) and the breakdown point (BP; Donoho & Huber, 1982). To the best of our knowledge, this is the first study to apply these tools in the context of neural density estimators and ABI.

### The Empirical Influence Function

When fitting parametric models, the data are assumed to follow a distribution  $F_{\theta}$  with unknown parameters  $\theta$ , where  $\theta$  can be estimated from a sample  $\mathbf{x} = \{x_1, \dots, x_n\}$ . Bayesian methods return a (possibly approximate) posterior  $p(\theta | \mathbf{x})$ , which can be summarized into a point estimate (e.g., a posterior mean). A point estimator of  $\theta$  is denoted as  $\hat{\theta}$  and the dependence of the estimator on  $\mathbf{x}$  is denoted as  $\hat{\theta}(\mathbf{x})$ . If the sample size  $n$  becomes very large (i.e.,  $n \rightarrow \infty$ ), then the information in the sample  $\mathbf{x}$  in fact converges to the information provided by the distribution  $F$ , and thus  $\hat{\theta}(F) \rightarrow \theta$ , assuming the estimator is consistent. However, outliers can contaminate the distribution. Denoting the contaminant distribution as  $G$  and the (small) fraction of contaminants as  $\epsilon$ , we can define the contaminated distribution as

$$F_{\theta}^{\epsilon, G} = (1 - \epsilon)F + \epsilon G. \quad (8)$$

In the study of the influence of outliers, the contaminant distribution is usually defined as a point mass  $G \equiv \delta_{x^c}$ , with

$$\delta_{x^c} = \begin{cases} 1 & \text{if } x = x^c \\ 0 & \text{otherwise,} \end{cases} \quad (9)$$

where  $x^c$  is the contaminant. Thus, we can define the influence function (IF; Maronna et al., 2006) for an estimator  $F(\hat{\theta})$  and an outlier  $x^c$  as:

$$\text{IF}_{\hat{\theta}}(x^c, F) = \lim_{\epsilon \rightarrow 0} \frac{\hat{\theta}((1 - \epsilon)F + \epsilon\delta_{x^c}) - \hat{\theta}(F)}{\epsilon}. \quad (10)$$

The IF indicates how much influence an outlier exerts on the estimate  $\hat{\boldsymbol{\theta}}$  asymptotically, thereby showing the sensitivity of the estimator to a particular value  $x^c$ . The influence function can be traced for a range of  $x^c$  values, and graphically represented. The result is the *influence curve* where the x-axis depicts the value of  $x^c$ , and the y-axis depicts the influence of  $x^c$  on  $\hat{\boldsymbol{\theta}}$ .

In practice, finding a closed-form expression for the IF of an estimator of an arbitrary  $F$  is hard. Instead, we can compute the Empirical Influence Function (Cook & Weisberg, 1980) (or “sensitivity curve” when represented graphically) to approximate the IF through simulations. Let us denote by  $\mathbf{x}^{c,i}$  a contaminated sample of finite size  $n$  (also called the perturbed data), where the  $i$ th observation of the original sample  $\mathbf{x}$  is replaced by the contaminant  $x^c$ . Because in this paper we only deal with permutation-invariant data, we can take  $i = 1$  without loss of generality. Therefore, we proceed with the notation  $\mathbf{x}^{c,1}$ , which indicates that the first component of the sample is replaced by  $x^c$ . The EIF is then defined as:

$$EIF(x^c, \mathbf{x}) = \hat{\boldsymbol{\theta}}(\mathbf{x}^{c,1}) - \hat{\boldsymbol{\theta}}(\mathbf{x}), \quad (11)$$

where  $\mathbf{x}$  are the original data from  $F$  and  $\mathbf{x}^{c,1}$  are the perturbed data. The EIF still depends on a single data set  $\mathbf{x}$  but we are not interested in this particular data set. Therefore, we will take the expected value  $\mathbb{E}[EIF(x^c, \mathbf{x})]$ , with respect to  $p(\mathbf{x}, \boldsymbol{\theta})$ . This expectation can be estimated using the sample average over  $B$  simulations:

$$\overline{EIF}(x^c) = \frac{1}{B} \sum_{b=1}^B EIF(x^c, \mathbf{x}^b),$$

with  $\mathbf{x}^b$  being the  $b$ th simulated sample. Again, by varying the value of  $x^c$ , we can plot a sensitivity curve for parameter estimates in the model, showing the relationship between the value of outliers and the difference it brings about in the parameter estimates. In the remaining part of the paper, we follow the convention in robust statistics literature, using EIF to represent the average EIF of an outlier across replications.

## The Breakdown Point

While the EIF assesses the sensitivity of parameter estimates to a single outlier, the BP is the minimum amount of contamination that can lead an estimator to produce extremely aberrant values (Donoho & Huber, 1982). A more precise definition is as follows. Assume that  $\Theta$  is parameter space for the parameter vector  $\boldsymbol{\theta}$  (i.e.,  $\boldsymbol{\theta} \in \Theta$ ). The asymptotic contamination BP  $\epsilon^*$  of the estimator  $\hat{\boldsymbol{\theta}}$  at  $F$  is the largest  $\epsilon^* \in (0, 1)$  such that for  $\epsilon < \epsilon^*$ ,  $\hat{\boldsymbol{\theta}}((1 - \epsilon)F + \epsilon\delta_{x^c})$  remains bounded away from the boundary of  $\Theta$  (Maronna et al., 2006). What this means is that the contamination should not drive the estimated parameter  $\hat{\boldsymbol{\theta}}$  to the boundary of  $\Theta$  (or to infinity if  $\Theta$  is unbounded for some or all of its components). A high BP means that  $\epsilon^*$  is large. For example, the BP of the median is 50%.

In a practical setting with a finite sample size  $n$ , we define a fraction  $p = \frac{m}{n}$ , so that

$m = p \cdot n$  observations in the sample  $\mathbf{x}$  are replaced by  $x^c$  (again, without loss of generality, we replace the first  $m$  entries). The contaminated sample can be denoted as  $\mathbf{x}^{c(p)}$ . This leads to an estimation  $\hat{\boldsymbol{\theta}}(\mathbf{x}^{c(p)})$ . Again, the sample average over  $B$  samples can be taken:  $\overline{\hat{\boldsymbol{\theta}}}(x^c, p)$ . The BP is then the fraction  $p^*$  for which all fractions  $p < p^*$  lead to an average estimate that is still acceptable:  $|\overline{\hat{\boldsymbol{\theta}}}(x^c, p) - \overline{\hat{\boldsymbol{\theta}}}| < \Delta$  (where  $\Delta$  is some tolerance).

## The Impact of Outliers in Amortized Estimation of the Mean of a Normal Distribution

Before applying the two key concepts from robust statistics to query the robustness of amortized DDM estimation, we study the EIF and BP in a toy example, investigating how outliers can influence the estimate of the mean  $\mu$ , where  $n$  i.i.d. samples are drawn from:

$$x_1, x_2, \dots, x_n \stackrel{\text{i.i.d.}}{\sim} \mathcal{N}(\mu, 1), \quad (12)$$

so that  $\mathbf{x} = \{x_1, \dots, x_n\}$ .

First, we train neural networks with simulated data according to Equation 12. The parameters  $\{\mu_j\}_{j=1}^J$  are sampled from a prior distribution  $\mathcal{N}(0, 1)$ , and for each  $\mu_j$ , 10 to 100 samples from  $\mathcal{N}(\mu_j, 1)$  are generated. The neural network architecture consists of a Deep Set network with a 2-dimensional out (Zaheer et al., 2017), and an inference network comprising two layers with an affine design. The network is trained for 10 epochs, with 4000 iterations per epoch and a batch size of 32. After training, we check the parameter recovery to confirm that the estimated posterior mean aligns almost perfectly with the analytical posterior mean (Gelman et al., 2013).

### Empirical Influence Function of Amortized Mean Estimator

We evaluate the impact of outliers with the EIF for  $n \in \{10, 20, 100\}$ . For each  $n$ , 500 new data sets are simulated. Next, the first observation in each data set is substituted with an outlier  $x^c$ . Subsequently, we compute the average difference in the estimated  $\mu$  across the 500 new data sets. We repeat this procedure while systematically varying the value of  $x^c$ , from  $-100$  to  $100$ , incrementing by 1. This systematic manipulation allows us to construct the average EIF to illustrate the relationship between outlier values and their impact. The sensitivity curve as graphical representation of the average EIF is shown in Figure 5.

For the toy example, we can compare the numerical obtained EIF with an analytical expression. As a starting point, take the least squares estimate of  $\mu$  for a sample with the

first observation replaced by  $x^c$ :

$$\begin{aligned}\hat{\mu}(\mathbf{x}^{c,1}) &= \frac{1}{n+1}(x^c + x_2 + \dots + x_n) \\ &= \frac{1}{n+1}x^c + \frac{1}{n+1}\sum_{i=2}^n x_i.\end{aligned}$$

The expression for the EIF is then:

$$\begin{aligned}EIF_{\hat{\mu}}(x^{c,1}, \mathbf{x}) &= \frac{1}{n+1}x^c + \frac{1}{n+1}\sum_{i=2}^n x_i - \frac{1}{n+1}\sum_{i=1}^n x_i \\ &= \frac{1}{n+1}x^c - \frac{1}{n+1}x_1.\end{aligned}$$

Consequently (averaging over  $x_1$  and  $\mu$ ),  $\overline{EIF}_{\hat{\mu}}(x^c) = \frac{1}{n+1}x^c - \frac{1}{n+1}\mu$ , demonstrating a linear relationship between  $x^c$  and the theoretical average empirical influence, with slope  $\frac{1}{n+1}$ . Since the prior is centered around zero, the intercept also takes the value of zero. Both the theoretical EIF and that obtained from the neural networks are shown in the left panel of Figure 5. This shows that the neural estimator behaves identically as the analytical posterior mean under the influence of an outlier.

### Breakdown point of Amortized Mean Estimator

In this section, we estimate the BP of the estimator using an extreme outlier value  $x^c = -100$ . The fraction of contamination is  $p$ , so that  $p \cdot n$  observations are replaced by  $x^c = -100$ , leading to a contaminated sample  $\mathbf{x}^{c(p)}$ . As in the previous section, for each  $p$ , we simulate 500 new data sets and compute the average estimated  $\bar{\hat{\mu}}(\mathbf{x}^{c(p)})$ . The average  $\bar{\hat{\mu}}(\mathbf{x}^{c(p)})$  can then be plotted as a function of the fraction of outliers  $p$ . This procedure repeats three times with  $n \in \{10, 20, 100\}$ .

Again, the BP is available analytically for this simple example:

$$\begin{aligned}\hat{\mu}(\mathbf{x}^{c(p)}) &= \frac{1}{n+1}(p \cdot n \cdot x^c + \sum_{i=n-p \cdot n}^n x_i) \\ &= \frac{n}{n+1}px^c + \frac{1}{n+1}\sum_{i=n-p \cdot n}^n x_i,\end{aligned}$$

such that averaging over the data  $\mathbf{x}$  and the parameter  $\mu$  yields:

$$\bar{\hat{\mu}}(\mathbf{x}^c, p) = \frac{n}{n+1}px^c$$

Thus, even for the smallest fraction  $p = \frac{1}{n}$ , the estimate can be made arbitrarily large by choosing an appropriate value for  $x^c$ .

As can be seen from the right panel in Figure 5, the ABI estimation of  $\mu$  depends linearly on the fraction of outliers in the sample (as also our derivation has shown).

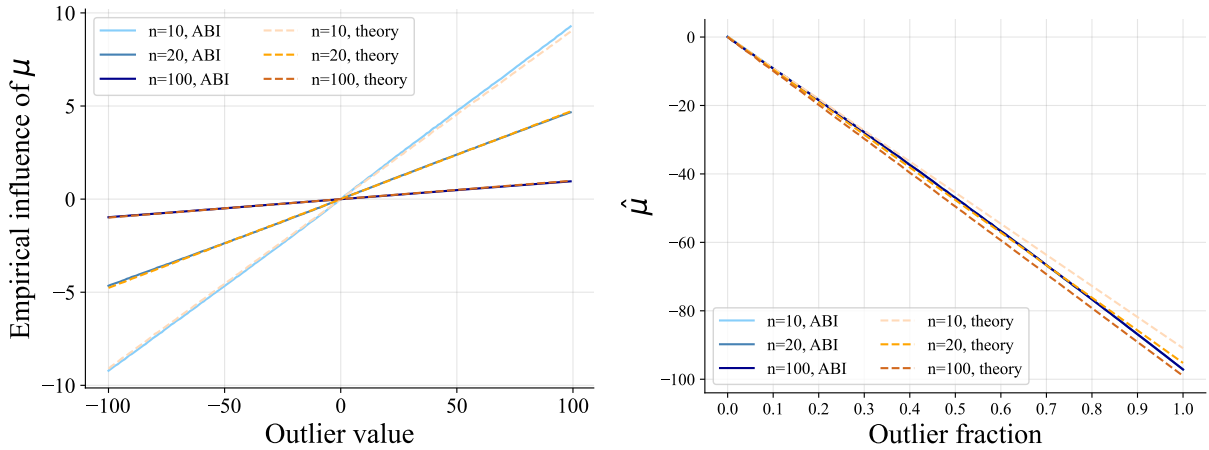


Figure 5: The EIF and BP for the  $\mu$  estimator when  $n \in \{10, 20, 100\}$ . The left panel shows the  $\overline{EIF}_{\hat{\mu}}(x^c)$  for the estimation of  $\mu$  in both theory and BayesFlow. The right panel shows the average estimate of  $\mu$  with a fraction of  $p$  outliers (i.e., copies of  $x^c = -100$ ) inserted into the sample (i.e.,  $\hat{\mu}(\mathbf{x}^c, p)$ ).

Therefore it is no surprise that the results from the theory and ABI align closely.

## The Impact of Outliers in Amortized DDM Parameter Estimation

This section explores the robustness of ABI for the DDM parameters through EIF and BP. Before discussing the results, we will first explain the specification of the neural networks, priors and training.

### Specification of the ABI for Estimating DDM Parameters

As explained before, we train the neural networks estimator using simulated choice reaction time data. Firstly, we sample parameters  $\{\boldsymbol{\theta}_1, \dots, \boldsymbol{\theta}_J\}_{j=1}^J$  from a prior (see Tables 4). In this simulation, we consider two distinct conditions leading to different decisions, each associated with a specific sign of the drift rate. These parameters are then input into an observation model to produce choice reaction time data:

$$(rt_i, y_i) \sim \text{Wiener}(v_i, a_i, z_i, T_{er,i}), \quad (13)$$

where the index  $i$  refers to the particular trial: for trials in condition 1, the drift rate is  $v_1$  and for trials in condition 2, it is  $v_2$ . Other parameters stay the same across trials. A complete data set is thus  $(\mathbf{rt}, \mathbf{y}) = \{(rt_1, y_1), \dots, (rt_n, y_n)\}$ . The number of trials  $n$  in each data set varies from 100 to 1000, which allows us after training to make inference on data sets with a wide range of number of trials.

The summary network is a Set Transformer (Lee et al., 2019) that outputs 12 summary statistics as output, while the inference network is a neural spline flow composed of six coupling layers. The training process runs for 100 epochs with 1000 iterations per epoch and a batch size of 32. The loss value converges successfully by the end of the training.



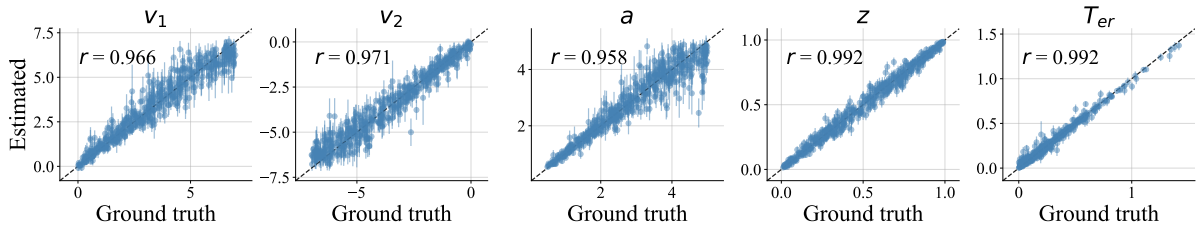


Figure 6: Parameter recovery of DDM parameters using BayesFlow on 500 new data sets with  $n = 500$  trials each. The error bars quantify the uncertainty by representing  $\pm$  posterior standard deviation around the point estimates.

Next, we simulate additional 500 data sets and perform parameter recovery (see Figure 3).

Table 3: Prior distributions over the DDM parameters.

Parameters	Distribution
$v_1$ (Drift Rate 1)	$U(0, 7)$
$v_2$ (Drift Rate 2)	$U(-7, 0)$
$a$ (Boundary Separation)	$U(0.1, 5)$
$z$ (Starting Point)	$U(0.01, 0.99)$
$T_{er}$ (Non-Decision Time)	$\text{Gamma}(1.5, 0.2)$

Table 4: Prior distributions over the DDM parameters.  $\text{Gamma}(1.5, 0.2)$  denotes a gamma distribution with shape parameter 1.5 and scale parameter 0.2.

### Empirical Influence Function of Amortized DDM Estimator

Next, we assess the impact of outliers on DDM estimates through the EIF. When introducing outliers into reaction time data, we assume that both the reaction time and response in a certain entry are affected. Thus, we not only replace the first reaction time with an outlier  $rt^c$ , but also sample the corresponding response  $y^c$  from a Bernoulli distribution with a probability of 0.5. The reasons for also altering  $y^c$  are: (1) we would like to study the influence of  $rt^c$  while averaging out the effect of the choices; (2) in practice, when there is an outlier in the data set, the corresponding choice is likely to be a random guess. In our numerical experiments,  $rt^c$  ranges from 0.01 to 20 seconds, increasing in increments of 0.05 seconds. For each  $rt^c$ , we generate 500 data sets with 100 trials each and compute the average difference in the parameter values estimated from the perturbed and original data.

Figure 7a shows the EIF for the five DDM parameters. To provide a more fine-grained analysis in the short outlier value range, as short outliers are expected to be particularly detrimental, we also plot the EIF of  $rt^c$  ranging from 0 to 1 second, with an increment of 0.01 seconds as in Figure 7b. The results illustrate that a single outlier significantly impacts the estimation of DDM parameters.

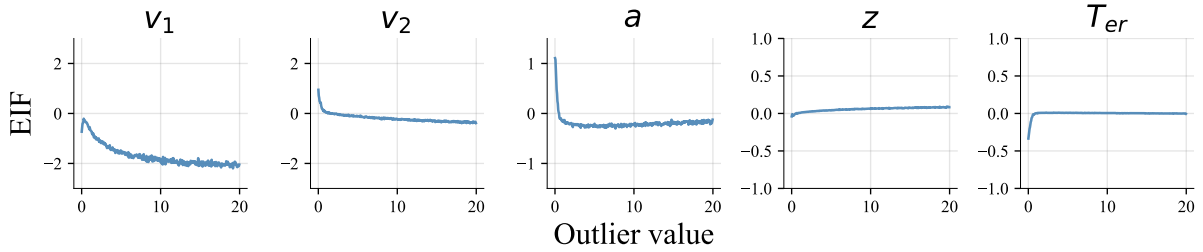
As expected, short outliers smaller than 0.5s generally lead to underestimated non-decision time  $T_{er}$ . As a result, the actual “decision time” is spuriously prolonged. This

has two effects. First, the information accumulation is assumed to be slower than the true state, resulting in underestimated drift rates. Second, it is assumed that more information is needed to reach a decision, resulting in an overestimated boundary separation  $a$ . On the other hand, longer outliers do not have as strong an effect on  $T_{er}$  as the short outliers. However, they still exert a notable impact, especially on the drift rate of the first condition, as an observation in this condition is altered. If the mean reaction time in a condition becomes longer, the information accumulation process is also assumed to be slower. Overall, both short and long outliers exhibit a significant influence on DDM estimates.

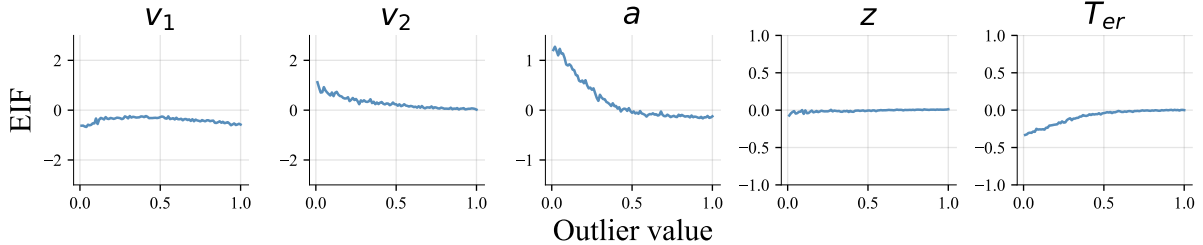
### Breakdown Point of Amortized DDM Estimator

We explore the BP of amortized DDM estimator by introducing a fraction  $p$  of contaminants with extreme values  $rt^c$  into the first condition, while treating the corresponding responses  $y^c$  as random guesses. For each  $p$ , we simulate and fit 500 additional data sets. By comparing the average posterior mean of the original data set with that of the perturbed data set, we identify the contamination level at which the estimator can still produce reliable inferences. The average posterior mean across hundreds of data sets is simply the prior mean (for priors, see Table 4), which is shown as the red dashed line in Figure 7c and 7d.

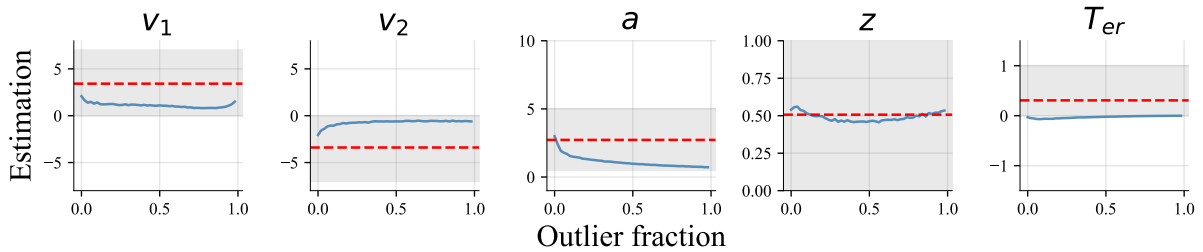
Figure 7c shows the BP results for short outliers ( $rt^c = 0.01s$ ), while Figure 7d shows the BP results for long outliers ( $rt^c = 20s$ ). On one hand, with more  $rt^c = 0.01s$  in the first condition, the drift rates in both conditions and the boundary separation approach zero. On the other hand, with more  $rt^c = 20s$  in the first condition,  $v_1$  is estimated to be near zero,  $v_2$  becomes more extreme, and the boundary separation approaches the upper boundary of its prior. In both cases (short and long outliers), the estimation becomes severely distorted starting at  $p^* = \frac{1}{n}$ , which is identified as the BP. In addition, in the presence of multiple short outliers, the estimator even produces negative posterior means for  $T_{er}$ , exceeding its boundaries as can be seen in Figure 7c. Overall, the BP plot reveals that the estimator is highly susceptible to contamination.



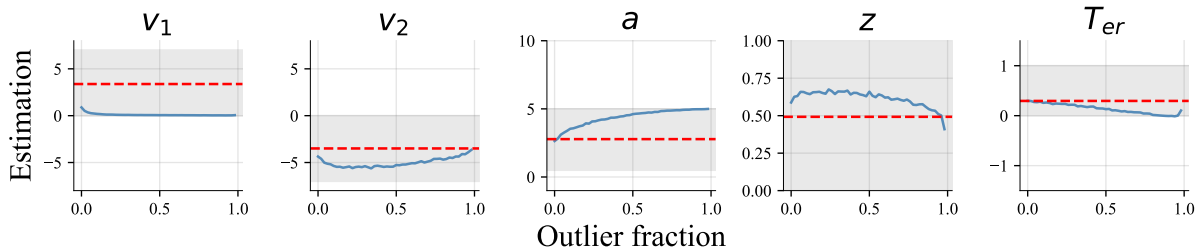
(a) EIF for the DDM parameters with  $rt^c$  from 0.01 to 20s.



(b) EIF for the DDM parameters with  $rt^c$  from 0.01 to 1s.



(c) BP for the DDM parameters with  $rt^c = 0.01s$  and contamination fraction  $p$ .



(d) BP for the DDM parameters with  $rt^c = 20s$  and contamination fraction  $p$ .

Figure 7: EIF and BP of amortized DDM estimation. Row (a) shows the EIF when  $rt^c$  ranges from 0.01s to 20s. Row (b) zooms in on the EIF when  $rt^c = 0.01 \sim 1s$ , with a higher resolution. Row (c) shows the BP of the estimator when  $rt^c = 0.01s$ , while row (d) shows that with large outliers, namely  $rt^c = 20s$ . The true posterior mean across 1000 data sets is the prior mean, which is indicated with the red dashed line. The grey area marks the prior density for this parameter. The deviation between the estimates of perturbed data sets (in blue line) and the red dashed line is the systematic bias that a certain fraction of outliers brings.

## Inspection of the Latent Space of the Amortized DDM Estimator

Posterior errors in amortized Bayesian inference due to outliers can be revealed by inspecting the latent space via simulations. In BayesFlow, the networks learn an invertible nonlinear mapping between the posterior  $p(\boldsymbol{\theta} | t(\mathbf{x}))$  and a (multivariate) Gaussian distribution. Thus, with good convergence, the latent space should approximate a spherical

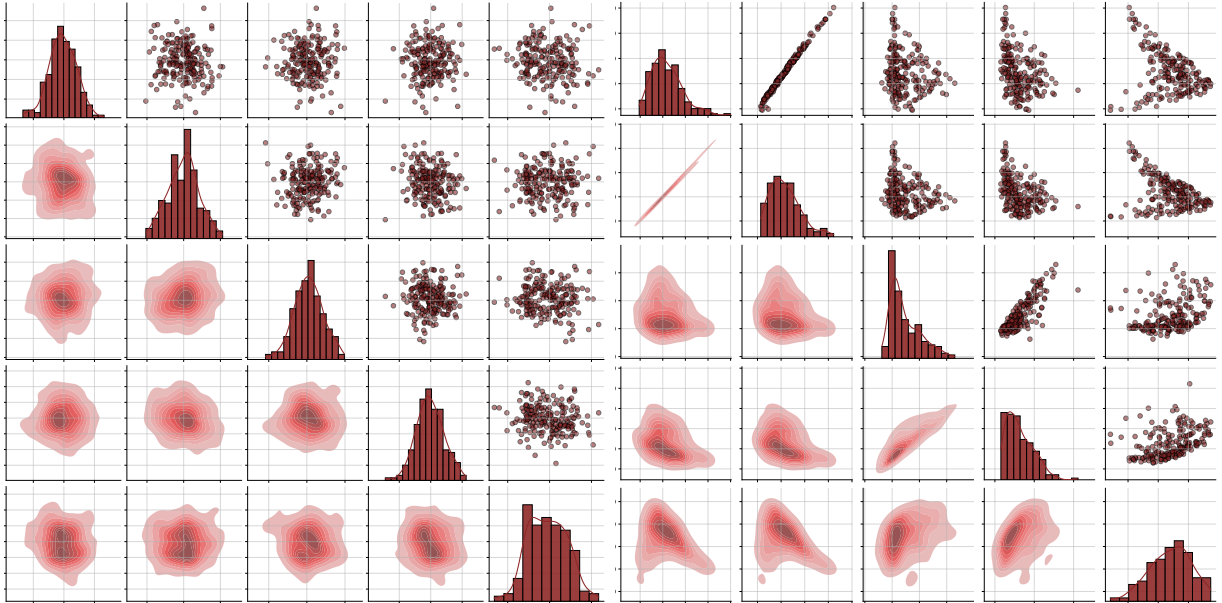


Figure 8: Latent space inspection. The left panel is the latent space of 100 data sets simulated from DDM without contamination, and the right panel is the latent space of 100 perturbed data set with  $rt^c = 0.01s$ . The uncontaminated data can be mapped to the prescribed multivariate Gaussian structure, while the contaminated data fails to be mapped to this structure because the networks have not learned the contaminated pattern.

Gaussian. This is illustrated in the left panel of Figure 8, where simulated DDM data are passed through the networks, and the resulting latent space closely resembles a Gaussian.

However, when we inject contaminants by replacing the first reaction time in each data set with  $rt^c = 0.01s$  and again plot the resulting latent space, we observe serious deviations from normality (see the right panel of Figure 8). Thus, sampling from a latent Gaussian and applying the inverse transformation would not yield samples from the true posterior (Siahkoohi et al., 2023). In other words, this occurs because the networks have not been trained to transform contaminated patterns. As such, inspecting the latent space can reveal distortions caused by data contamination or model misspecification in simulation studies (i.e., when ground truth parameters are available).

# Robustify Amortized Bayesian Inference: Training with Perturbed Data

In previous sections, the network was trained with simulated data that strictly adhered to the model assumptions. This led to estimation problems when outliers were present in the data. However, ABI can be made more robust by introducing contaminants in the simulator and thus exposing the networks to outliers during training. In the remainder of this paper, we refer to the estimator trained with perfectly clean data as the *non-robust* or *standard estimator*, and the estimator trained with contaminated data as the *robust estimator*. Despite the conceptual simplicity of this approach, several concerns may arise, such as (1) whether it truly produces robust results or (2) whether different contamination distributions impact parameter estimation. We attempt to answer these questions within both the normal toy example and the DDM.

## Robustify Amortized Estimation of the Mean of a Normal Distribution

For the standard estimator in the normal toy example, we assumed that the data come from an uncontaminated model (i.e., a normal distribution) as in Equation 12. For the robust estimator, we will replace the normal distribution with a contaminated observation model  $\mathbf{x}^c$ :

$$\mathbf{x}^c \sim \begin{cases} \mathcal{N}(\mu, 1), & \text{with probability } 1 - \pi \\ t_\nu(\mu, 1), & \text{with probability } \pi, \end{cases} \quad (14)$$

where  $t_\nu(\mu, 1)$  refers to a  $t$  distribution with location  $\mu$ , scale 1 and degrees of freedom  $\nu$ , and  $\pi$  is a predefined contamination probability. In the case of the normal toy example, we set it to be 0.1. In the remainder, we train three estimators with  $\nu \in \{1, 3, 5\}$ , respectively, exploring the difference in estimation.

We train the three robust estimators with the same settings as in the standard  $\mu$  estimator, except for the epochs: the robust estimators with  $t_3$  and  $t_5$  are trained for 15 and 20 epochs, respectively. The reason is for robust estimator with  $t_3$  and  $t_5$ , the network is less likely to encounter outliers during the training phase (see Table 5). Therefore, we allow for longer training. The prior and sample sizes in the observation model are the same as in training the standard  $\mu$  estimator in the previous section. After training, 500 new sets of data are simulated to perform a parameter recovery check for each estimator (Figure 9).

Next, we assess the robustness of these estimators and explore their differences. We first generate the EIF plots for all the robust estimators. The procedure is the same as mentioned above in assessing robustness for the standard  $\mu$  estimator. The results are shown in the left panel of Figure 10, which should be compared to the left panel of Figure 5 (note the different scales of the y-axis). Around the origin there is a linear

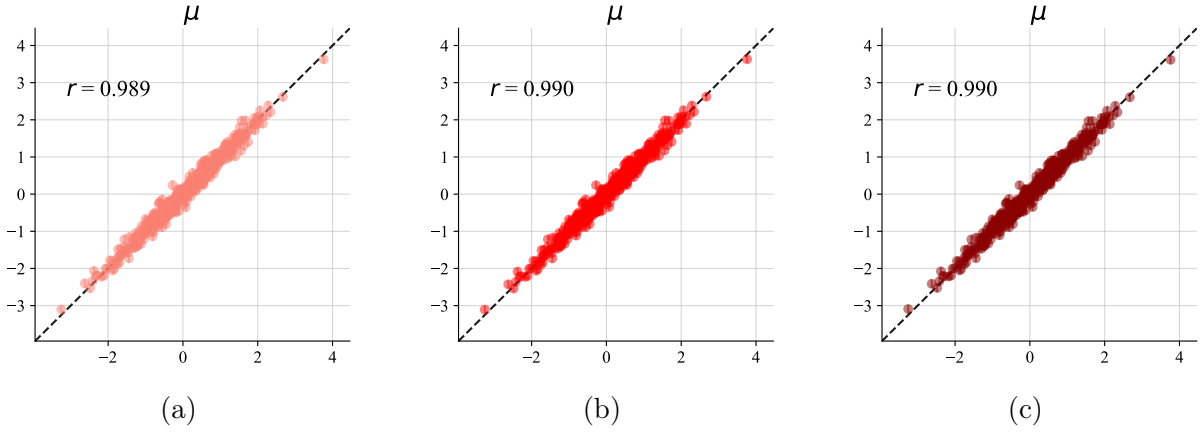


Figure 9: Parameter recovery of  $\mu$  for robust neural estimators. The contamination distributions in each estimator are  $t_\nu(\mu, 1)$ , where  $\nu = 1$  in Panel (a),  $\nu = 3$  in Panel (b) and  $\nu = 5$  in Panel (c). 500 new data sets are simulated from the standard simulator with  $n = 20$ .

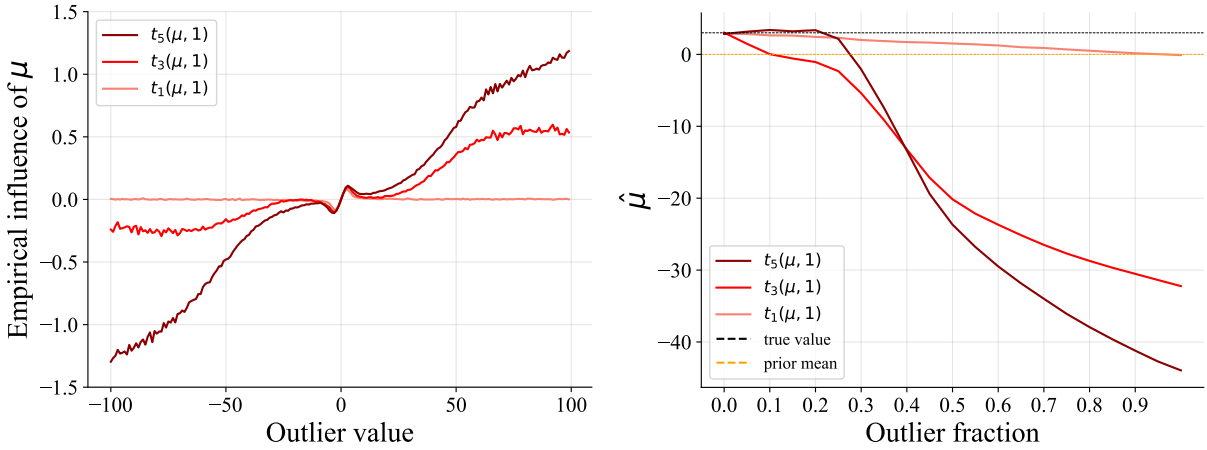


Figure 10: EIF and BP of robust neural estimators of  $\mu$  trained with different degrees of freedom  $\nu$ .

dependence on  $x^c$ , while in a region further away from the origin (thus for more extreme values of  $x^c$ , the influence is down weighted. For the robust  $t_1$  estimator, the influence becomes effectively zero across the whole range while the  $t_3$  and  $t_5$  robust estimators show some increased influence for very extreme values. The latter is most likely due to extrapolation because during training the estimator has not been confronted with such extreme values. Table 5 shows the percentage of regular and far outliers (Tukey, 1977) under each of the contaminant distributions used in the various robust estimators (and the normal distribution added for comparison). It can be seen that under 10% contamination with the  $t_1$  distribution, regular and far outliers occur considerably more frequent.

Let us compare the behavior of the neural robust  $t_1$  estimator to some analytical results from robust statistics. Tukey's biweight function is an example of an  $M$ -estimator of location proposed in robust statistics (Tukey, 1979). The resulting influence function

is as follows:

$$\text{IF}_{\hat{\mu}}(x^c, F) = \begin{cases} (1 - (x^c/k)^2)^2, & \text{if } |x^c| \leq k \\ 0 & \text{if } |x^c| > k, \end{cases} \quad (15)$$

where  $k$  is a tuning constant or a cutoff value that ensures the estimator becomes insensitive to contaminants in absolute value larger than  $k$ . This influence function has some desirable theoretical properties (see e.g., Hampel et al., 2005). We can overlay the graph of the empirical influence function from the robust  $t_1$  neural estimator with the graph of the influence function of Tukey’s biweight loss function (taking  $k = 6$ ) as is done in Figure 11. The two graphs show a high degree of overlap, which suggests that the robust  $t_1$  neural estimator operates similarly to traditional robust estimators developed under the MLE framework.

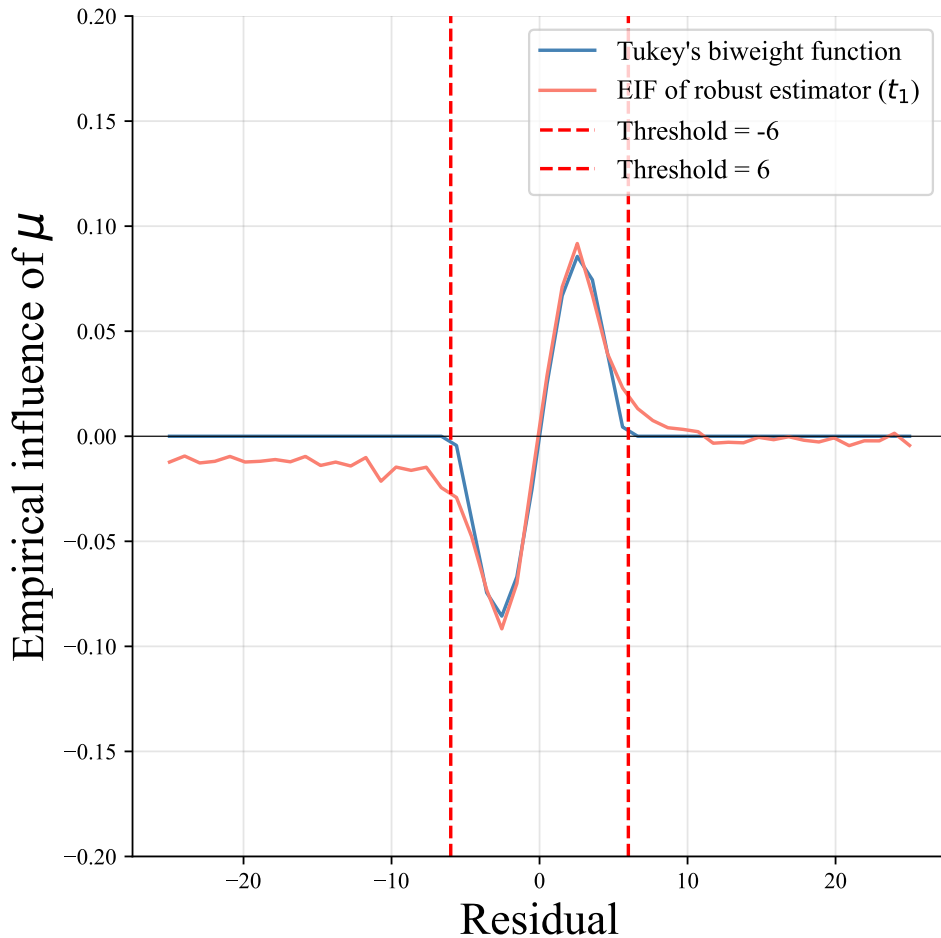


Figure 11: Influence function with Tukey’s biweight loss function and EIF of robust neural estimator of  $\mu$  trained with  $\nu = 1$ .

In a next step, we assess the BP of the estimators. As before, we contaminate the clean data set with increasing amounts of contamination (taking  $x^c = -100$  as contaminant) and compute the average estimate  $\hat{\mu}$  across 500 data set for the three robust estimators. In order to get a nuanced idea of the breakdown point for each estimator, we will not average of the prior on  $\mu$ . The reason for this choice is that if the robust estimators revert to the mean of the prior (which is zero) when breaking down, we will not be able

to detect this because they were already originally estimating zero. Therefore, we take as the ground truth value  $\mu = 3$ . An estimator that is robust to contaminants should show an average estimated mean  $\hat{\mu}$  close to the true mean  $\mu = 3$ . As the right panel of Figure 10 shows, the robust estimator with  $\nu = 1$  in the contamination distribution exhibits the highest resistance to contamination, and as  $\nu$  increases, the breakdown point becomes smaller. When a data set is full of  $x^c = -100$ , the estimation converges the prior mean, which is 0, indicating the networks no longer take any information from the data.

Estimator		Regular outliers		Far outliers	
		$Q_3 + 1.5 \cdot IQR$	%	$Q_3 + 3 \cdot IQR$	%
Robust	normal + 10% $t_1$	2.828	2.585	4.949	1.269
	normal + 10% $t_3$	2.734	1.280	4.785	0.174
	normal + 10% $t_5$	2.719	1.008	4.758	0.051
Standard	normal	2.698	0.698	4.721	0.0002

Table 5: Percentage of regular and far outliers under three contaminated simulators (with  $\pi = .1$ ) and the standard normal simulator. Regular outliers are data points beyond 1.5 times the interquartile range (IQR) from the lower and upper quartiles (i.e.,  $Q_1$  and  $Q_3$ , respectively), while far outliers are those beyond 3 times the IQR from the quartiles (Tukey, 1977). This table shows the percentage of regular and far outliers in different simulators, as well as the threshold of them. Only the the upper boundaries are shown because the distributions we use in simulators are symmetric.

Overall, assuming a contaminated observation model significantly enhances the robustness in estimating  $\mu$ , and  $t_1$  performs best among our candidate contamination distributions.

## Robustify Amortized DDM Estimation

To robustify the neural density estimator for DDM, we produce contaminated data  $(\mathbf{rt}^c, \mathbf{y}^c)$  as follows:

$$(\mathbf{rt}^c, \mathbf{y}^c) \sim \begin{cases} \text{Wiener}(v, a, z, T_{er}), & \text{with probability } 1 - \pi \\ G, & \text{with probability } \pi \end{cases} \quad (16)$$

with  $\pi = 0.1$ .

To study the effect of different contamination distributions  $G$ , we train four distinct robust estimators, where  $rt^c$  are drawn from a folded- $t_\nu$  distribution (i.e., the absolute value of  $t$  distributed random variable) or from a uniform distribution between 0s and 20s. At the same time, in a contaminated trial, the corresponding response is assumed to



come from a Bernoulli distribution with a probability of 0.5, implying random guessing:

$$rt_i^c \sim \begin{cases} \text{folded-}t_1 & \text{or} \\ \text{folded-}t_3 & \text{or} \\ \text{folded-}t_5 & \text{or} \\ U(0, 20) \end{cases}$$

and

$$y_i^c \sim \text{Bern}(0.5).$$

Figure 12 shows the histogram of perfectly clean reaction time data (for a variety of parameter vectors; in blue) overlaid with the density of the different contamination distributions.

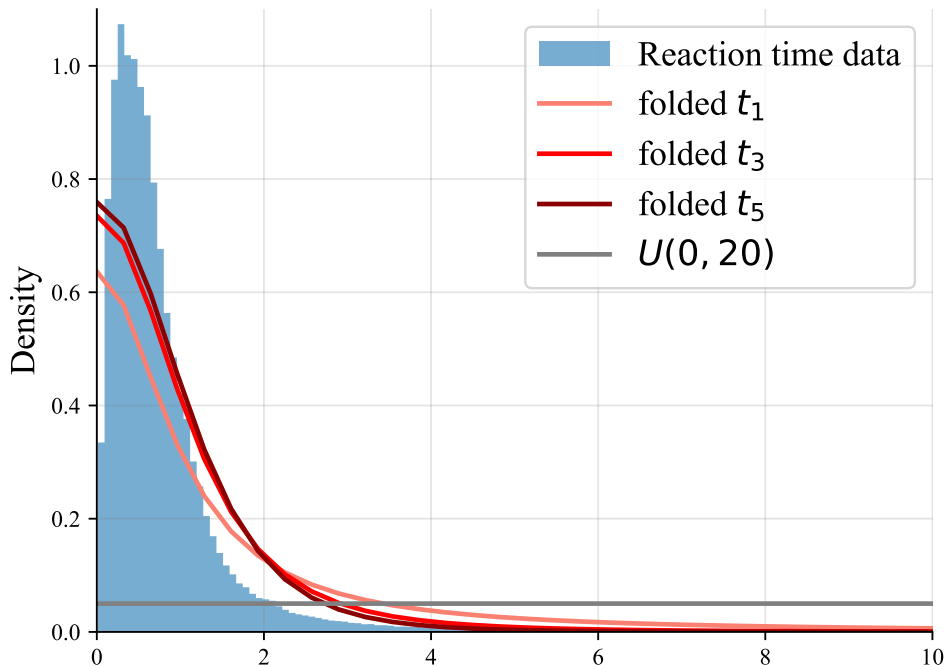


Figure 12: Histogram of reaction times generated by the DDM for a sample of 500 parameter vectors from the prior overlaid with the densities of the four contamination distributions.

As before, we train four robust estimators with contaminated data, using the same sample sizes, network structure and training epochs as in the training of a standard DDM estimator. The loss values decrease and converge for all the robust estimators. As depicted in Figure 13, all the robust estimators accurately recover the parameters.

After assessing recovery, we evaluate the performance of robust estimators using the EIF. Overall, as can be seen from Figure 14, all four robust estimators demonstrate resistance to both short and long outliers (Figure 14 should be compared to Figure 7). However, the robust estimator with a uniform distribution shows the greatest bias from short outliers in both drift rate and boundary separation estimates. This occurs because,

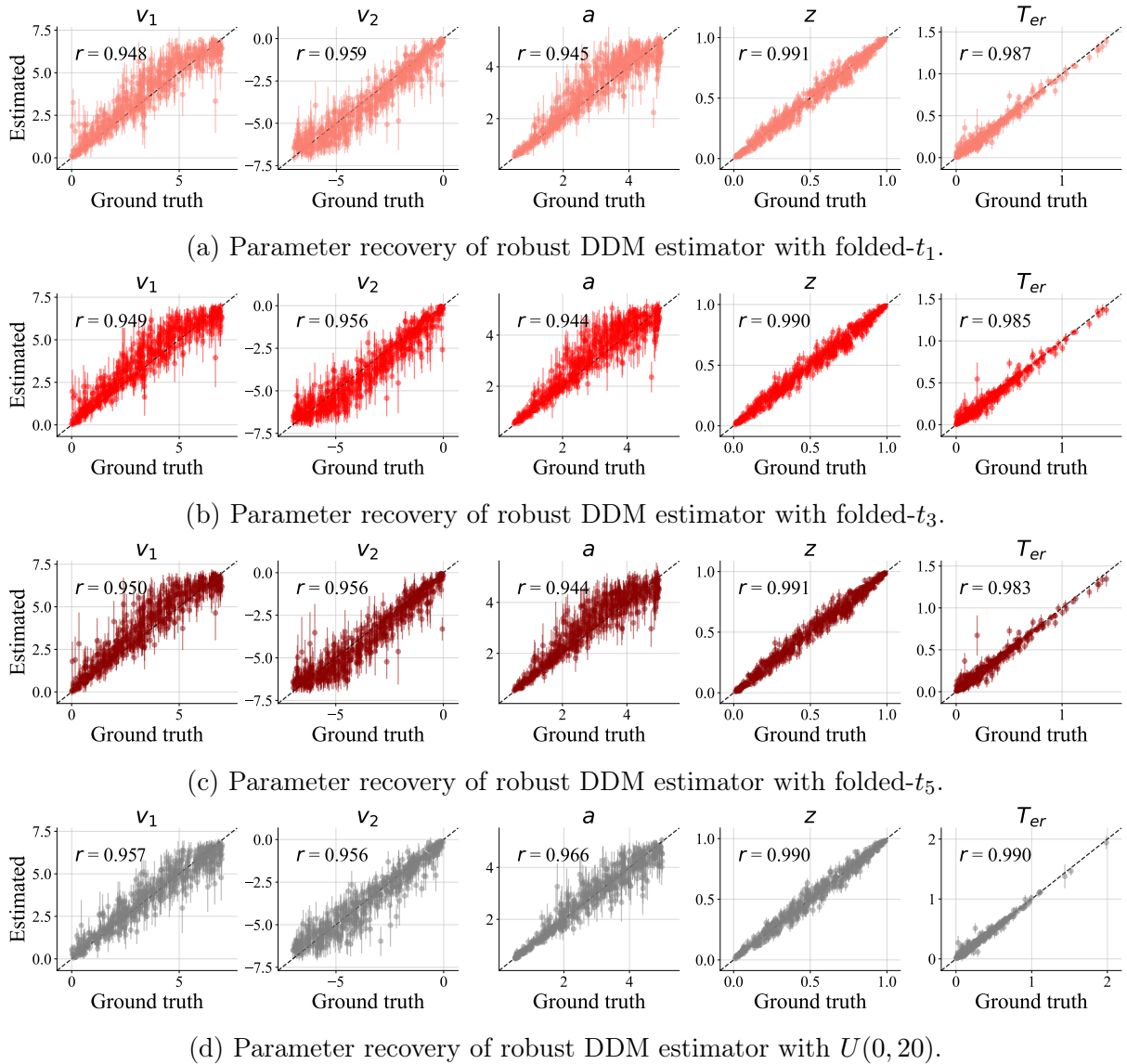
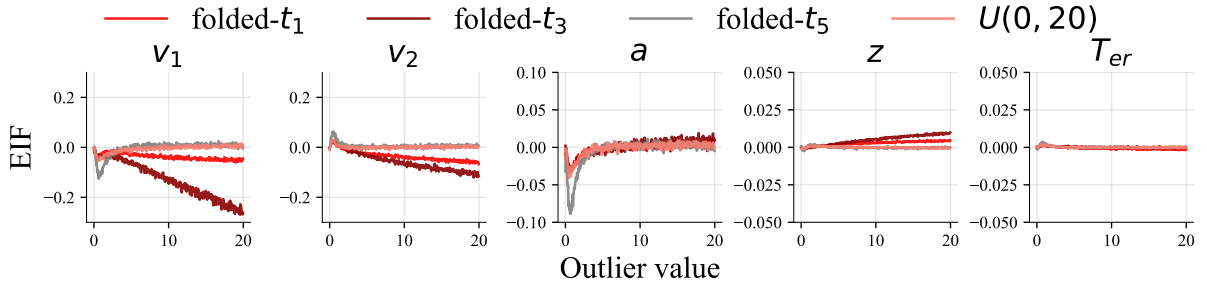


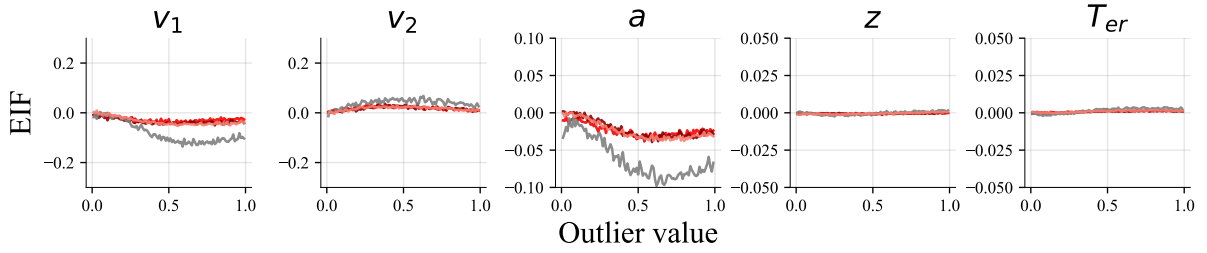
Figure 13: Parameter recovery of robust DDM estimators on 500 new data sets when the total trial number  $n = 100$  (50 per condition). The 500 new data set are simulated from the standard DDM simulator without any contamination.

unlike  $t$  distributions which are centered around 0 and place high weights on short outliers, the uniform distribution assigns less weights to short outliers. Among the estimators using  $t$  distributions, we find again that the lower the degrees of freedom  $\nu$ , the better the performance in mitigating the influence of long outliers. This is due to the heavier tails of distributions with low degrees of freedom, which increase the likelihood of encountering extreme reaction times during training, allowing the network to learn to filter them out.

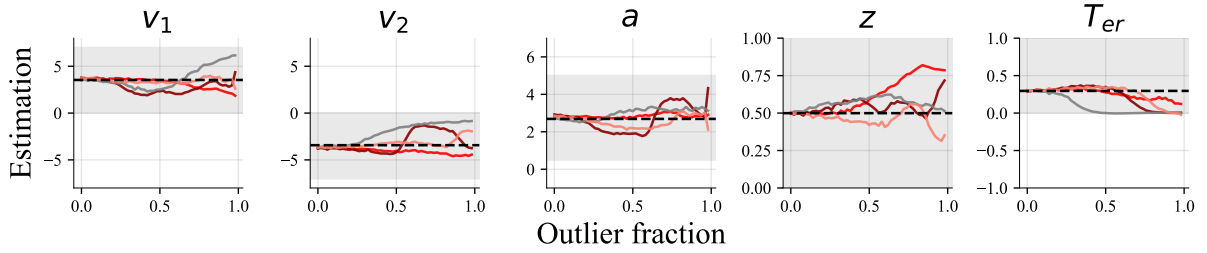
The properties of the different robust estimators are also evident from their BPs. We test the BP with  $rt^c = 0.01s$  and  $rt^c = 20s$ , respectively, and manipulate the contamination fraction  $p$  in the first condition, from  $\frac{1}{50}$  to  $\frac{50}{50}$ . The results are shown in Figure 14c and Figure 14d. The three robust estimators with  $t$  distributions assign similar weight to numbers around 0, while the uniform distribution assigns equal weight across 0 to 20. Consequently, when  $rt^c = 0.01s$ , the robust estimator with a uniform distribution has the low-



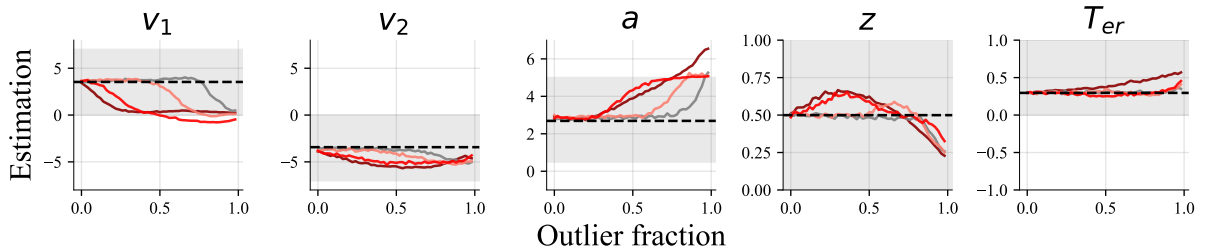
(a) EIF for DDM parameter in robust estimators with  $rt^c$  from 0.01 to 20s.



(b) EIF for DDM parameter in robust estimators with  $rt^c$  from 0.01 to 1s.



(c) BP for DDM parameters in robust estimators with  $rt^c = 0.01s$  and contamination fraction  $p$ .



(d) BP for DDM parameters in robust estimators with  $rt^c = 20s$  and contamination fraction  $p$ .

Figure 14: EIF and BP of robust neural estimators (applied to data sets with two conditions and 50 trials per condition). Panels in the top row (a) show the EIF when  $rt^c = 0.01 \sim 20s$ . Panels in the second row (b) are a zoom-in of the EIF when  $rt^c = 0.01 \sim 1s$ , with a higher resolution. Panels in row (c) display the BP of the estimator when  $rt^c = 0.01s$ , while panels in row (d) show the BP with large outliers ( $rt^c = 20s$ ). For the BP graphs in rows (c) and (d) the true ground truth value across 1000 data sets is indicated with the black dashed line. The grey area marks the prior density for this parameter. The deviation between the estimates of perturbed data sets and the black dashed line is the systematic bias that a certain fraction of outliers brings.

est BP, compared to the other robust estimators. The situation is reversed for  $rt^c = 20s$ , where the weight assigned to the tail follows  $U(0, 20) > \text{folded-}t_1 > \text{folded-}t_3 > \text{folded-}t_5$ . It is important to note that  $U(0, 20)$  is an artificial distribution with arbitrary cutoffs, and  $rt^c = 20s$  is an exceptionally rare value in empirical datasets. Thus, we conclude that the robust estimator with a  $t_1$  distribution performs the best among all robust estimator, and the lower the  $\nu$ , the higher the contamination threshold that can induce severe bias.

In summary, incorporating a contaminated observation model during training leads to more robust estimators for the DDM parameters. Additionally, the choice of contamination distribution has a significant impact on the estimator’s performance. In both toy example and DDM,  $t_1$  contamination distribution shows best performance among all the candidates. Based on this result, additional exploratory simulations with varying contamination probabilities  $\pi$  in the  $t_1$  distribution is provided in the Appendix.

## The Cost of Robustness

It is well understood that there are trade-offs associated with any robust approach (Maronna et al., 2006). For example, robust M-estimators often exhibit efficiency losses, which refer to a higher asymptotic variance of the robust estimator compared to the standard estimator when there is no contamination in the datasets (Hampel et al., 2005). In this section, we explore the cost of the robust neural density estimator, evaluating (for the  $j$ th parameter  $\theta_j$ ) the accuracy and efficiency of a robust estimator  $\hat{\theta}_j^R$  compared to a standard estimator  $\hat{\theta}_j^S$ .

As a measure for accuracy, we compute the ratio of mean absolute error (MAE) as follows:

$$\text{MAE Ratio}_j^{S,R} = \frac{1}{B} \sum_{b=1}^B \frac{|\hat{\theta}_j^S(\mathbf{x}_b) - \theta_{j(b)}|}{|\hat{\theta}_j^R(\mathbf{x}_b) - \theta_{j(b)}|}, \quad (17)$$

where  $\mathbf{x}_b$  is the  $b$ th data set simulated from the standard model,  $\theta_{j(b)}$  is the true  $j$ th parameter value for  $b$ th data set, and  $B$  is the total number of data sets.

For efficiency loss, we use the ratio of average posterior variance:

$$\text{Posterior Variance Ratio}_j^{S,R} = \frac{1}{B} \sum_{b=1}^B \frac{\text{var}(\hat{\theta}_j^S | \mathbf{x}_b)}{\text{var}(\hat{\theta}_j^R | \mathbf{x}_b)}, \quad (18)$$

where  $\text{var}(\hat{\theta}_j | \mathbf{x}_b)$  is the variance of the marginal posterior distribution of the  $j$ th parameter based on the  $b$ th simulated data set  $\mathbf{x}_b$ .

## The Cost of Robustness in Mean Estimation

When estimating  $\mu$  in the normal toy example, we propose four different estimators (i.e., the standard ABI estimator and three robust estimators with contamination distributions  $t_1$ ,  $t_3$ , and  $t_5$ , respectively). We simulate 20000 data sets (each with a sample size of

$n = 20$ ) from the standard model with no contamination assumed, then fit the data using the four neural density estimators, and calculate the two ratios of interest (thus comparing each robust estimator to the standard estimator). The results are shown in Table 6. All the error ratios are close to 1, indicating minimal loss (0.1% to 0.2%) in accuracy when applying robust estimators to standard data. However, the variance ratios reveal notable efficiency losses in robust estimators. Specifically, the robust  $\mu$  estimator with  $t_1$  exhibits the highest level of efficiency loss, around 9.0%. This level of efficiency loss is comparable to the efficiency loss observed in M-estimators for finite samples ( $n = 20$ ) when estimating  $\mu$  in a univariate normal distribution (Wu, 1985). For example, the Hampel, Huber, and Tukey’s biweight ( $k = 6$ ) M-estimators show efficiency losses of 4.8%, 17.0%, and 11.2% compared to the optimal least-squares estimator, respectively. Our robust estimators with  $t_1$ ,  $t_3$ , and  $t_5$  show 9.0%, 5.5%, and 3.3% efficiency losses compared to a standard neural  $\mu$  estimator, respectively. This demonstrates that the robust neural  $\mu$  estimator, especially the one with  $t_1$ , is highly robust and still efficient. Meanwhile, as  $\nu$  increases, the efficiency loss continues to decrease. This shows a clear robustness-efficiency trade-off: the robust estimator with higher  $\nu$  is also found to be more robust against outliers, as shown in Figure 10.

Table 6: MAE and posterior variance ratios of the three robust neural estimators for  $\mu$ . Each row compares the robust estimator to the standard estimator.

Robust estimator	MAE Ratio	Posterior Variance Ratio
$t_1$	0.999	0.910
$t_3$	0.998	0.945
$t_5$	0.999	0.967

## The Cost of Robustness in DDM Estimation

The robust neural estimators of the DDM parameters are inherently more complex and multidimensional compared to estimator of the single  $\mu$  parameter. We evaluate the accuracy and efficiency loss under ideal conditions (no contaminants) of four robust neural estimators (i.e.,  $t_1$ ,  $t_3$ ,  $t_5$ , and  $U(0, 20)$ ), each compared to the standard DDM estimator.

We simulate 10000 data sets ( $n = 100$ ) and calculate the ratios of the MAE (see Equation 17) and posterior variance (see Equation 18) compared to the standard estimator. The results are shown in Tables 7 and 8, respectively. As expected, also for the robust DDM estimator, the accuracies are lower for all the robust estimators (e.g., depending on the parameter, about 12% to 24% loss in accuracy for the robust estimator based on the  $t_1$  distribution) compared to the standard one. No systematic relationship between  $\nu$  and performance of the estimators is detected. The robust estimator with  $U(0, 20)$  has less accuracy loss (from around 6% to 15% for the five parameters). However, at the same time, it is the least robust against short outliers among all robust estimators (see Figure 14).

In terms of efficiency loss, all robust estimators exhibit a moderate to high loss, with values reaching up to 43% for the  $T_{er}$  parameter in the robust estimator with folded- $t_1$ . However, the efficiency loss in DDM is not comparable to that in estimating  $\mu$  as the models differ in complexity and parameter interdependency. The high cost of achieving robustness in estimating a complex model can be mitigated by decreasing the contamination probability  $\pi$  during the training of the robust neural network (for a simulation demonstrating the effect of  $\pi$ , please refer to the Appendix). Naturally, this adjustment again represents a trade-off between robustness and efficiency, as decreasing  $\pi$  results in an estimator with a lower BP, as shown in Figure A4.

Table 7: MAE ratios of the four robust neural DDM estimators. Each row compares the robust estimator to the standard estimator.

Robust estimator	$v_1$	$v_2$	$a$	$z$	$T_{er}$
$t_1$	0.76	0.79	0.769	0.88	0.792
$t_3$	0.731	0.722	0.728	0.865	0.764
$t_5$	0.728	0.74	0.734	0.862	0.733
$U(0, 20)$	0.876	0.894	0.907	0.936	0.848

Table 8: Posterior variance ratios of the four robust neural DDM estimators. Each row compares the robust estimator to the standard estimator.

Robust estimator	$v_1$	$v_2$	$a$	$z$	$T_{er}$
$t_1$	0.613	0.596	0.621	0.732	0.571
$t_3$	0.637	0.569	0.634	0.694	0.581
$t_5$	0.618	0.569	0.672	0.713	0.568
$U(0, 20)$	0.723	0.672	0.723	0.756	0.636

## Real Data Example

All of the above numerical experiments involved simulations. In this section, we apply our robust training to the data set from (Ratcliff & Rouder, 1998), available as `rr98` in the R package `RTDists` (Singmann et al., 2022)). The goal of this real life example is to demonstrate the practicality of the robust approach. We fit the raw data set using both standard and robust neural estimators with BayesFlow to explore differences in estimation. Additionally, we fit an outlier-cleaned version of the data and again compare both estimators.

In this experiment, three participants were asked to decide whether the overall brightness of pixel arrays displayed on a computer monitor was “bright” or “dark”. The experiment is a  $33 \times 2$  within-subject design. One factor is the brightness strength which has 33 levels (array with 0% white pixels to 100% white pixels), and the other factor was the instruction, indicating whether participants needed to respond as quickly as possible

(i.e., speed instruction) or as accurately as possible (i.e., accuracy instruction). This is a typical manipulation in decision tasks and was designed to study the speed-accuracy trade-off in decision-making. Each participant contributed approximately 4,000 trials per instruction condition.

Firstly, the data set is preprocessed. We simplify the analysis and interpretation by grouping the 33 levels in brightness strength into five strength bins. As the speed and accuracy instructions could impact boundary separation and other parameters, we separate the data and fit two independent DDMs. This approach follows the methods in Ratcliff and Rouder (1998) and Singmann (2022).

Secondly, we explore the data distribution by plotting them. We plot the proportion of “dark” response against the strength bins, as Figure 15 shows. This plot clearly indicates a strong effect of brightness strength on response choice. Additionally, we examine response times across five quantiles (i.e., 10%, 30%, 50%, 70%, and 90%) for each strength level, separating the plots by condition. As expected, the speed condition resulted in significantly shorter response times. These plots reveal substantial differences between the two instruction conditions (see Figure 16).

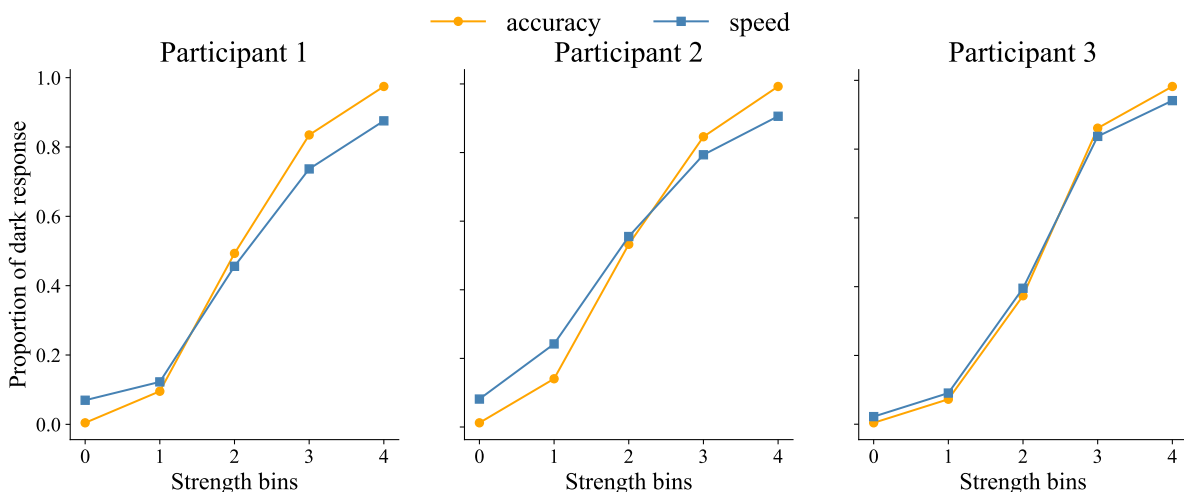


Figure 15: The relationship between proportion of “dark” responses and the brightness strength bins.

The standard estimator was trained on uncontaminated choice reaction time data, whereas the robust estimator was trained using a folded- $t_1$  as the contamination distribution, assuming a 10% probability of one data point being contaminated. The network architectures and training parameters were identical as in previous section, but sample size in each batch vary in trial numbers (from 100 to 5,000), allowing the model to remain expressive for up to around 4,000 trials. The model training was conducted using an NVIDIA Tesla V100-SXM2-32GB GPU due to the large number of simulations. Each epoch took approximately 95 seconds, resulting in a total training time of 158 minutes per network.

The raw and cleaned data are fed to the two networks. The cleaned data are obtained

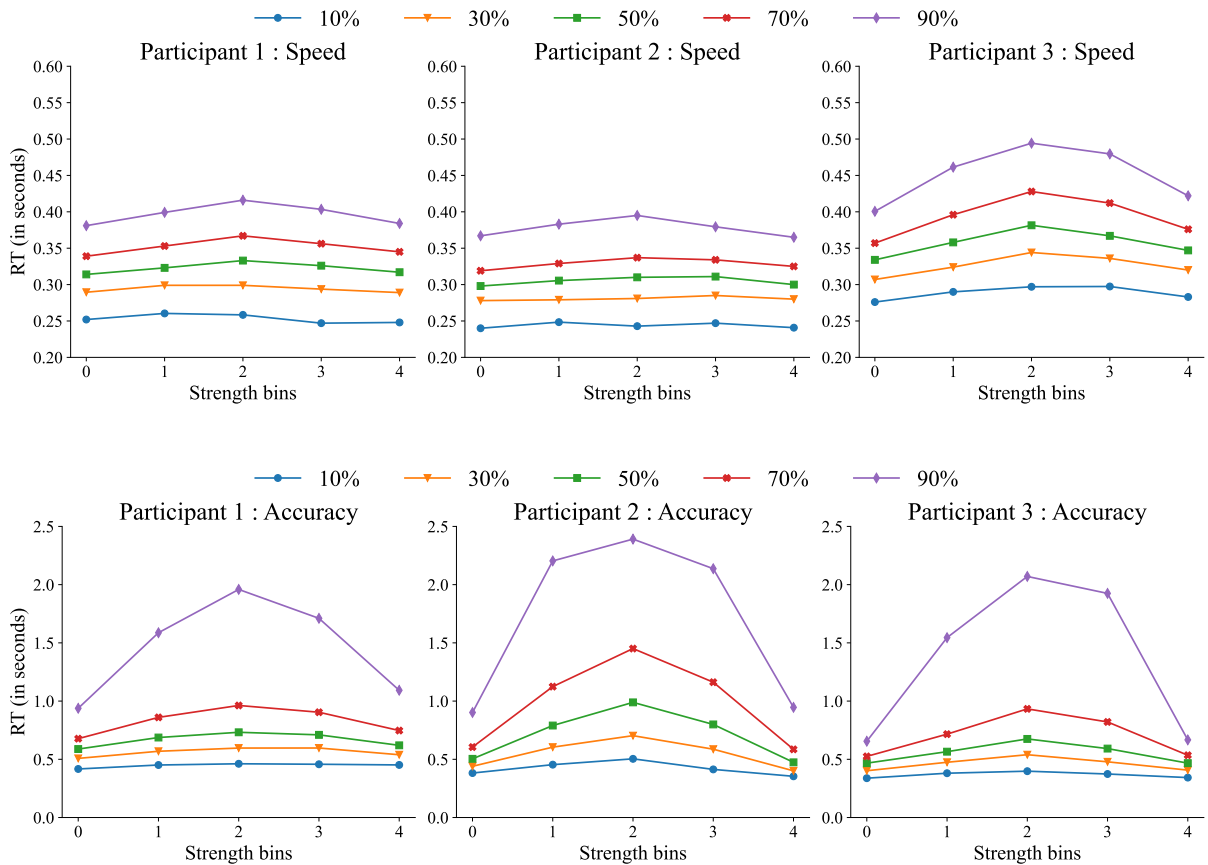


Figure 16: Quantile plot of reaction time. The upper panel shows the reaction time quantiles when participants were instructed to respond as fast as possible, while the lower panel displays the reaction time quantiles when participants were instructed to respond as accurately as possible.



by applying the original procedure for data cleaning outlined by Ratcliff and Rouder (1998), which involved discarding observations with reaction times shorter than 200 ms or longer than 2500 ms.

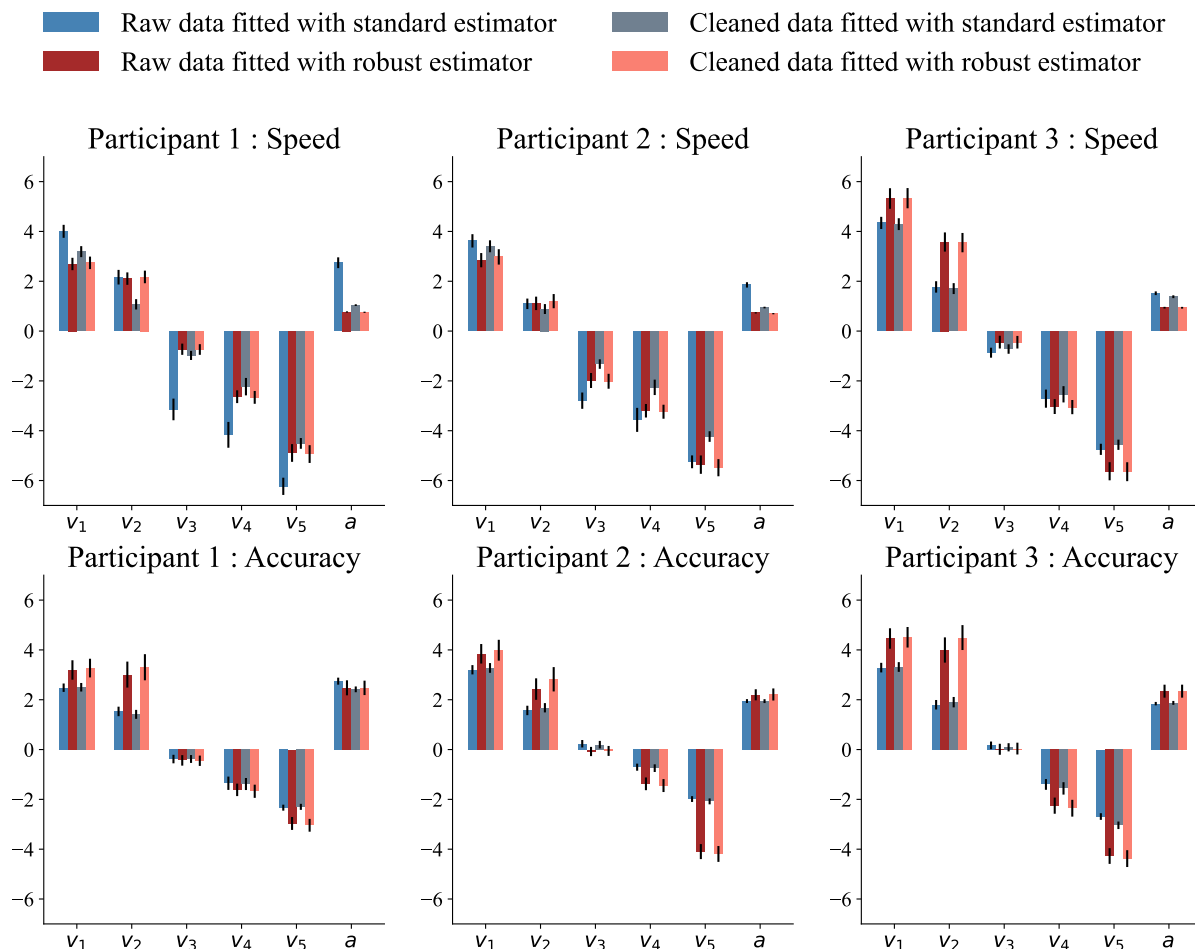


Figure 17: Inference of drift rate and boundary separation across different data sets and estimators. The y-axis represents the estimated values, while the x-axis shows the parameter names. The error bar represents one posterior standard deviation. These parameters are displayed in a single figure due to their similar scales.

For both networks and data sets, the posterior means and standard deviations are calculated and visualized in Figure 17 and Figure 18 (together with the posterior standard deviation). For inference under the speed instruction, the difference between raw or cleaned data fitted with the standard estimator makes a rather large difference (especially for participant 1 and 2). For the accuracy instruction data and the standard estimator, the difference between raw and cleaned data is less substantial. This is because, in the accuracy condition, most outliers are long outliers (95% fall between 2.52s and 6.98s), and we cannot conclude whether they are contaminants not stemming from the decision-making process (participants may hesitate to make a decision when being asked to be as accurate as possible). Such long outliers, whether present or absent in the data set, have a smaller impact parameter inference compared to short outliers. Under the speed instruction, most outliers are short (95% fall between 0.123s and 0.199s), and their pres-

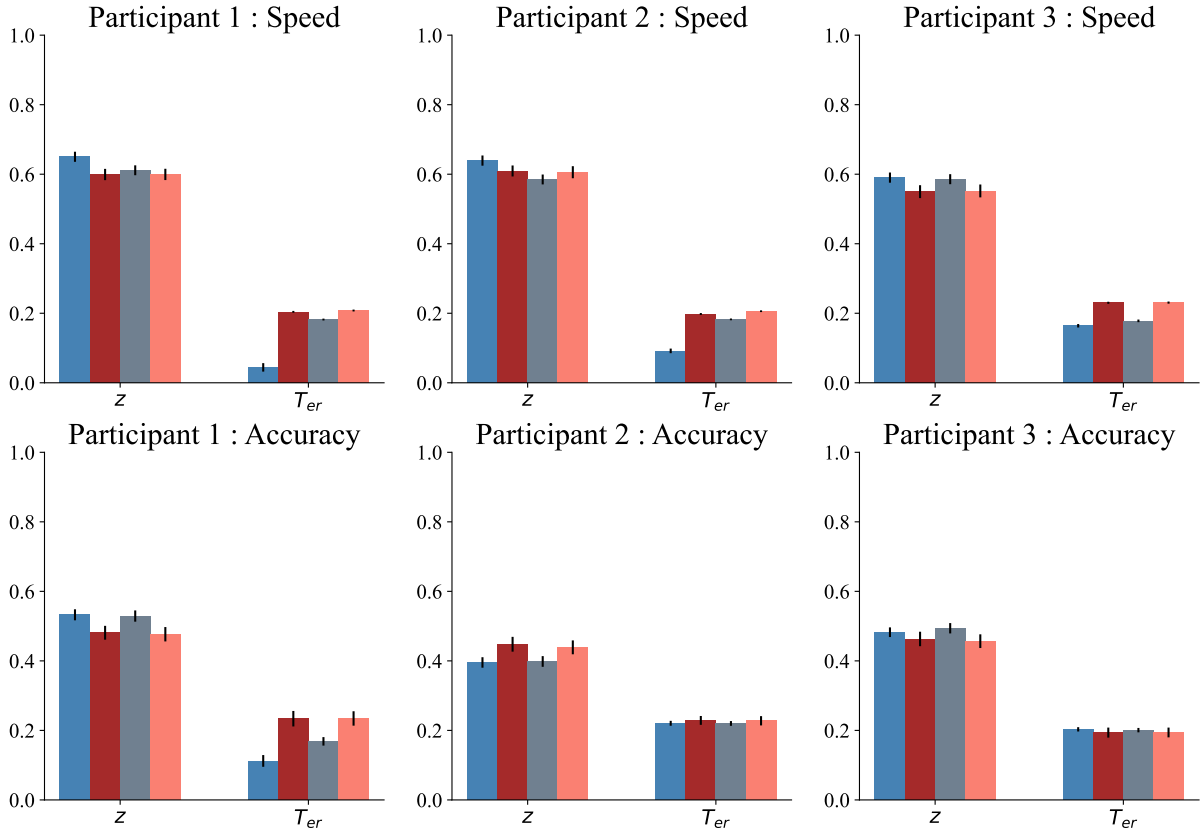


Figure 18: Inference of response bias and non-decision time across different data sets and estimators. The y-axis represents the estimated values, while the x-axis shows the parameter names. The error bar represents one standard deviation in posterior distribution. These parameters are displayed in a single figure due to their similar scales.

ence or absence in the data set leads to significant differences in estimation, as shown in Figure 17 and Figure 18. For the robust estimator, inputting raw or cleaned data does not affect the estimation strongly.

Since real data do not come with ground-truth parameters, we can only evaluate the degree to which the estimates reflect the effects of the factors in the experimental design. Parameters  $v_1$  to  $v_5$  correspond to conditions where the proportion of white pixels varies, with  $v_1$  representing the condition with the fewest white pixels in an array and  $v_5$  representing the condition with the most white pixels. Since the ‘dark’ response is the upper bound, it is reasonable to expect the following ordinal relationships:  $v_1 > v_2 > v_3 > v_4 > v_5$  under both speed and accuracy instructions, with  $v_3$  being the one closest to zero, as the information was most noisy and difficult to accumulate. This relationship was captured by the robust estimator applied to the raw data.

Meanwhile, the non-decision time in the standard estimator with the raw data set was severely underestimated for participants 1 and 2 in the speed condition due to the presence of short outliers. This underestimation leads to biases in other estimates, such

as overestimated drift rates and boundary separation (see Figure 7a and 17). The bias in boundary separation is particularly evident when comparing boundary separations under speed and accuracy instructions. Speed instructions are known to be associated with a lower boundary separation (Ratcliff, 1978; Ratcliff & Rouder, 1998; Ratcliff et al., 2016), as participants are less cautious when making decisions. This expected difference is reflected in the robust estimates. However, in the standard estimator, when the raw data were fitted, this difference was not observed, leading to biased conclusions.

In general, it holds for these data that robust estimators effectively capture expected relationships in data as induced by the manipulations, such as the ordinal ranking of conditions under experimental designs, while avoiding biases introduced by outliers. In contrast, standard estimators fail to account for outliers, leading to underestimation of non-decision time and overestimation of key parameters, causing misleading conclusions. Importantly, the robust neural estimator under ABI shows its advantages and high accessibility in real data application.

## Discussion

This paper focuses on the robustness of amortized Bayesian inference (ABI) for cognitive models with BayesFlow (Radev et al., 2020). ABI leverages simulations to train neural networks capable of compressing data of varying sizes and sampling from the posterior distribution of model parameters for any dataset compatible with the model (Zammit-Mangion et al., 2024). The systematic study of robustness in cognitive modeling can be challenging, as it is resource-intensive and time-consuming with traditional estimation methods, such as MCMC sampling (Wabersich & Vandekerckhove, 2014). However, ABI can accelerate such studies enormously, since the computational effort for estimating model parameters is “pre-paid” during training, and the estimator can be queried instantly on new data (Radev et al., 2020; Schumacher et al., 2023).

Thus, this study provides the first systematic exploration of the robustness of ABI, combining theoretical analysis and empirical assessment. Meanwhile, we offer a novel and straightforward method for robustifying ABI, making it a practical tool for a wide range of applications. The ability to handle outliers effectively while maintaining computational efficiency opens new doors for deploying ABI in real-world research scenarios.

We first demonstrated ABI’s ability in accurate estimation with a parameter recovery study of Drift Diffusion Model (DDM), and unpacked the blackbox of the summary statistics learned by the neural network. We found that the learned summary statistics in BayesFlow contains the same information as the summary statistics being used in EZ diffusion (Wagenmakers et al., 2007) which are sufficient to estimation. These findings position ABI as a method capable of maintaining interpretability while leveraging deep neural networks.

Then, we assessed the impact of outliers in ABI with a toy example (estimating  $\mu$  in

a normal distribution) and DDM with established tools in robust statistics, namely the empirical influence function (EIF) and breakdown point (BP). For  $\mu$  estimation, the EIF and BP in MLE and in BayesFlow nicely coincides. For DDM estimates, we show that one single outlier already leads to bias in estimation, and this sensitivity to outliers is due to the nature of DDM assumptions. These results highlight that the ABI is not robust to outliers when being trained by standard simulated data, and its sensitivity to outliers is similar to MLE. Thus, it is necessary to robustify ABI to ensure accuracy in outlier-prone data sets.

To improve the robustness of ABI, we proposed a simple yet very effective data augmentation method. Since we use simulated data to train the neural networks, by assuming a fraction of the data (e.g. 10%) comes from the contamination distribution during network training, allowing the neural networks to learn the mapping between contaminated data and a global posterior distribution. We examined contamination distributions based on  $t$  distributions with different degrees of freedom  $\nu$  and a uniform distribution. In both location parameter and DDM estimation, we found that assuming contamination arising from a  $t$  distribution with one degree of freedom (i.e., a Cauchy) largely improves robustness. Meanwhile, the robust neural  $\mu$  estimator with Cauchy distribution exhibits the same EIF as the Tukey’s Biweight function (Tukey, 1979), an M-estimator that apply transformations on residuals when using traditional least square method. This results imply that adding noise in the simulation part can achieve similar effects as manually manipulate the loss function, without having to rely on complicated mathematical arguments. This data augmentation method is a very straightforward approach that addresses a crucial methodological gap by integrating robust statistics with amortized inference.

As with all robust methods in statistics, robust ABI comes with a cost in efficiency. Compared to a standard estimator, a robust estimator exhibits higher variance in the posterior distribution when applied to uncontaminated data. We compare the efficiency losses in robust  $\mu$  estimator with robust statistics literature (Hampel et al., 2005; Tukey, 1979; Huber, 1964) and found that the robust  $\mu$  estimator with Cauchy distribution is both highly robust and efficient. However, efficiency losses in the robust DDM estimator lack a direct reference point (e.g., robust DDM estimators in robust statistics), making it difficult to evaluate whether the efficiency losses for such a complex model are at a low level. Meanwhile, we found there is a robustness-efficiency trade-off in neural density estimator, as same as in robust statistics (Hampel et al., 2005): the higher the robustness, the larger the efficiency losses. That is to say, the efficiency loss level can be managed by replacing the contamination distribution or simply decreasing the assumed fraction of data coming from the contamination distribution in data simulation. The results from efficiency losses in neural density estimator align closely with principles from robust statistics, paving the way to integrate these two research domains.

Lastly, we demonstrated the feasibility of applying our robust approach to real datasets. Our results suggest that the robust estimator with a Cauchy distribution is a highly

robust and practical method that holds significant potential for application in research areas where outlier detection or removal is particularly challenging.

At the same time, we acknowledge the limitations of current work. The first limitation is that, although we mainly work with  $t$  distribution in our two examples and found that the Cauchy distribution performs the best in terms of reducing influence of outliers while maintaining acceptable efficiency losses, the choice of contamination distribution is flexible and depend on the specific model and data. This principle is also illustrated in our own work because when working with reaction time data, it was a folded- $t_1$  distribution that gave good results. The choice of contamination distribution requires the researcher to have a general idea of the range of contaminants. Secondly, the probability  $\pi$  of one entry in the data set being contaminated during network training is determined by researcher, which again requires knowledge about the empirical data set. A possible extension would involve treating  $\pi$  as a parameter that can vary across data sets during data simulation, so that it can be estimated and used as an index of data quality. Such an approach can also lead to more efficient estimation for datasets that have a lower fraction of outliers. However, estimating  $\pi$  could be challenging in cases where the fraction of contaminants is small or when the contamination model differs significantly from the assumed one. Another possible future research direction concerns optimizing the neural architecture or post-training correction (Siahkoochi et al., 2023) with respect to the robustness of inference.

In conclusion, as ABI is a powerful method in terms of high flexibility and low computational cost in inference, assessing and robustifying the method facilitates both methodological development and practical application. This work paves the way for a new era of robust and efficient Bayesian inference, extending the applicability of ABI to complex real-world datasets.

## Conflicts of Interest

The authors declare no conflict of interest.

## Author Contributions

**Yufei Wu:** Methodology, software, data curation, formal analysis, writing—original draft. **Stefan Radev:** Resources, software, methodology, writing—reviewing and editing. **Francis Tuerlinckx:** Conceptualization, methodology, supervision, writing—reviewing and editing.

## Funding

Yufei Wu and Francis Tuerlinckx are partially supported by a grant from the Research Council of KU Leuven (C14/23/062).

## Data Availability

All data and code are available in the following repository: <https://github.com/yufeiwu1011/Robust-Amortized-Bayesian-Inference>

## Acknowledgments

We thank Kristof Meers for his assistance in accelerating the simulation code for the diffusion model.

## References

- Aggarwal, C. C. (2017). *Outlier Analysis*. Springer International Publishing. <https://doi.org/10.1007/978-3-319-47578-3>
- Ahn, W.-Y., Haines, N., & Zhang, L. (2017). Revealing neurocomputational mechanisms of reinforcement learning and decision-making with the hBayesDM package. *Computational Psychiatry*, 1, 24–57. doi:10.1162/CPSY\_a\_00002
- Ardizzone, L., Lüth, C., Kruse, J., Rother, C., & Köthe, U. (2019). *Guided Image Generation with Conditional Invertible Neural Networks*. <http://arxiv.org/abs/1907.02392>. arXiv:1907.02392 [cs]
- Cook, R. D. & Weisberg, S. (1980). Characterizations of an Empirical Influence Function for Detecting Influential Cases in Regression. *Technometrics*, 22(4), 495–508. <https://doi.org/10.1080/00401706.1980.10486199>
- Cranmer, K., Brehmer, J., & Louppe, G. (2020). The frontier of simulation-based inference. *Proceedings of the National Academy of Sciences*, 117(48), 30055–30062.
- Dax, M., Wildberger, J., Buchholz, S., Green, S. R., Macke, J. H., & Schölkopf, B. (2023). Flow matching for scalable simulation-based inference. *arXiv preprint arXiv:2305.17161*.
- Donoho, D. & Huber, P. (1982). The notion of breakdown point. *A Festschrift for Eric Lehmann*, 157–184. Wadsworth.
- Durkan, C., Bekasov, A., Murray, I., & Papamakarios, G. (2019). Neural spline flows. *Advances in Neural Information Processing Systems*, 32.
- Gelman, A., Carlin, J. B., Stern, H. S., Dunson, D. B., Vehtari, A., & Rubin, D. B. (2013). *Bayesian Data Analysis* (third ed.). Chapman and Hall/CRC Texts in Statistical Science Series. CRC. <https://stat.columbia.edu/~gelman/book/>

- Gelman, A. & Rubin, D. B. (1992). Inference from Iterative Simulation Using Multiple Sequences. *Statistical Science*, 7(4). <https://doi.org/10.1214/ss/1177011136>
- Gonçalves, P. J., Lueckmann, J.-M., Deistler, M., Nonnenmacher, M., Öcal, K., Bassetto, G., Chintaluri, C., Podlaski, W. F., Haddad, S. A., Vogels, T. P., et al. (2020). Training deep neural density estimators to identify mechanistic models of neural dynamics. *eLife*, 9, e56261.
- Hampel, F. R., Ronchetti, E. M., Rousseeuw, P. J., & Stahel, W. A. (2005). *Robust Statistics: The Approach Based on Influence Functions* (1 ed.). Wiley Series in Probability and Statistics. Wiley. <https://doi.org/10.1002/9781118186435>
- Hawkins, D. (1980). *Identification of Outliers*. Monographs on Statistics and Applied Probability Ser. Springer Netherlands.
- Huang, D., Bharti, A., Souza, A., Acerbi, L., & Kaski, S. (2024). Learning robust statistics for simulation-based inference under model misspecification. *Advances in Neural Information Processing Systems*, 36.
- Huber, P. J. (1964). Robust estimation of a location parameter. *The Annals of Mathematical Statistics*, 35(1), 73–101. <https://doi.org/10.1214/aoms/1177703732>
- Kelly, R., Nott, D. J., Frazier, D. T., Warne, D., & Drovandi, C. (2024). Misspecification-robust sequential neural likelihood for simulation-based inference. *Transactions on Machine Learning Research*, 2024(June), Article–number.
- Kobyzev, I., Prince, S. J., & Brubaker, M. A. (2020). Normalizing flows: An introduction and review of current methods. *IEEE Transactions on Pattern Analysis and Machine Intelligence*, 43(11), 3964–3979.
- Kruschke, J. K. (2011). *Doing Bayesian data analysis: a tutorial with R and BUGS*. Academic Press.
- Kullback, S. & Leibler, R. A. (1951). On Information and Sufficiency. *The Annals of Mathematical Statistics*, 22(1), 79–86. <https://doi.org/10.1214/aoms/1177729694>
- Lee, J., Lee, Y., Kim, J., Kosiorek, A., Choi, S., & Teh, Y. (2019). Set transformer: A framework for attention-based permutation-invariant neural networks.
- Lerche, V. & Voss, A. (2016). Model complexity in diffusion modeling: Benefits of making the model more parsimonious. *Frontiers in Psychology*, 7, 1324.
- Lerche, V., Voss, A., & Nagler, M. (2017). How many trials are required for parameter estimation in diffusion modeling? a comparison of different optimization criteria. *Behavior Research Methods*, 49, 513–537.

- Lipman, Y., Chen, R. T., Ben-Hamu, H., Nickel, M., & Le, M. (2022). Flow matching for generative modeling. *The Eleventh International Conference on Learning Representations*.
- Maniaci, M. R. & Rogge, R. D. (2014). Caring about carelessness: Participant inattention and its effects on research. *Journal of Research in Personality*, 48, 61–83. <https://doi.org/10.1016/j.jrp.2013.09.008>
- Maronna, R. A., Martin, R. D., & Yohai, V. J. (2006). *Robust Statistics: Theory and Methods* (1 ed.). Wiley Series in Probability and Statistics. Wiley. <https://doi.org/10.1002/0470010940>
- Mulder, M. J., Wagenmakers, E.-J., Ratcliff, R., Boekel, W., & Forstmann, B. U. (2012). Bias in the Brain: A Diffusion Model Analysis of Prior Probability and Potential Payoff. *The Journal of Neuroscience*, 32(7), 2335–2343. <https://doi.org/10.1523/JNEUROSCI.4156-11.2012>
- Myers, C. E., Interian, A., & Moustafa, A. A. (2022). A practical introduction to using the drift diffusion model of decision-making in cognitive psychology, neuroscience, and health sciences. *Frontiers in Psychology*, 13, 1039172. <https://doi.org/10.3389/fpsyg.2022.1039172>
- Radev, S. T., Mertens, U. K., Voss, A., Ardizzone, L., & Köthe, U. (2020). BayesFlow: Learning complex stochastic models with invertible neural networks. <https://doi.org/10.48550/ARXIV.2003.06281>. Publisher: arXiv Version Number: 4
- Radev, S. T., Schmitt, M., Schumacher, L., Elsemüller, L., Pratz, V., Schälte, Y., Köthe, U., & Bürkner, P.-C. (2023). BayesFlow: Amortized Bayesian Workflows With Neural Networks. *Journal of Open Source Software*, 8(89), 5702. <https://doi.org/10.21105/joss.05702>
- Ratcliff, R. (1978). A theory of memory retrieval. *Psychological Review*, 85(2), 59–108. <https://doi.org/10.1037/0033-295X.85.2.59>
- Ratcliff, R. (1993). Methods for dealing with reaction time outliers. *Psychological Bulletin*, 114(3), 510–532. <https://doi.org/10.1037/0033-2909.114.3.510>
- Ratcliff, R., Gomez, P., & McKoon, G. (2004). A Diffusion Model Account of the Lexical Decision Task. *Psychological Review*, 111(1), 159–182. <https://doi.org/10.1037/0033-295X.111.1.159>
- Ratcliff, R. & Rouder, J. N. (1998). Modeling Response Times for Two-Choice Decisions. *Psychological Science*, 9(5), 347–356. <https://doi.org/10.1111/1467-9280.00067>



- Ratcliff, R., Smith, P. L., Brown, S. D., & McKoon, G. (2016). Diffusion Decision Model: Current Issues and History. *Trends in Cognitive Sciences*, 20(4), 260–281. <https://doi.org/10.1016/j.tics.2016.01.007>
- Ratcliff, R. & Tuerlinckx, F. (2002). Estimating parameters of the diffusion model: Approaches to dealing with contaminant reaction times and parameter variability. *Psychonomic Bulletin & Review*, 9(3), 438–481. <https://doi.org/10.3758/BF03196302>
- Schad, D. J., Betancourt, M., & Vasishth, S. (2021). Toward a principled bayesian workflow in cognitive science. *Psychological Methods*, 26(1), 103.
- Schmitt, M., Bürkner, P.-C., Köthe, U., & Radev, S. T. (2021). *Detecting Model Misspecification in Amortized Bayesian Inference with Neural Networks*. <https://doi.org/10.48550/ARXIV.2112.08866>. Version Number: 5
- Schmitt, M., Li, C., Vehtari, A., Acerbi, L., Bürkner, P.-C., & Radev, S. T. (2024a). Amortized Bayesian workflow. *NeurIPS 2024 Workshop on Bayesian Decision-making and Uncertainty*.
- Schmitt, M., Pratz, V., Köthe, U., Bürkner, P.-C., & Radev, S. T. (2024b). Consistency models for scalable and fast simulation-based inference. *Advances in Neural Information Processing Systems (NeurIPS)*.
- Schumacher, L., Bürkner, P.-C., Voss, A., Köthe, U., & Radev, S. T. (2023). Neural superstatistics for Bayesian estimation of dynamic cognitive models. *Scientific Reports*, 13(1), 13778. <https://doi.org/10.1038/s41598-023-40278-3>
- Segal, M. & Xiao, Y. (2011). Multivariate random forests. *WIREs Data Mining and Knowledge Discovery*, 1(1), 80–87. <https://doi.org/10.1002/widm.12>
- Siahkoohi, A., Rizzuti, G., Orozco, R., & Herrmann, F. J. (2023). Reliable amortized variational inference with physics-based latent distribution correction. *Geophysics*, 88(3), R297–R322.
- Simons, J., Sharrock, L., Liu, S., & Beaumont, M. (2023). Neural score estimation: Likelihood-free inference with conditional score based diffusion models. *Fifth Symposium on Advances in Approximate Bayesian Inference*.
- Singmann, H. (2022). *Reanalysis of Ratcliff and Rouder (1998) with Diffusion Model and LBA*. [https://cran.r-project.org/web/packages/rtdists/vignettes/reanalysis\\_rr98.html#description-of-the-experiment](https://cran.r-project.org/web/packages/rtdists/vignettes/reanalysis_rr98.html#description-of-the-experiment)
- Singmann, H., Brown, S., Gretton, M., Heathcote, A., Voss, A., Voss, J., & Terry, A. (2022). *rtdists: Response Time Distributions*. <https://cran.r-project.org/web/packages/rtdists/index.html>. R package version 0.11.5

- Spaniol, J., Madden, D. J., & Voss, A. (2006). A diffusion model analysis of adult age differences in episodic and semantic long-term memory retrieval. *Journal of Experimental Psychology: Learning, Memory, and Cognition*, 32(1), 101–117. <https://doi.org/10.1037/0278-7393.32.1.101>
- Sumarni, C., Sadik, K., Notodiputro, K. A., & Sartono, B. (2017). Robustness of location estimators under  $t$ -distributions: a literature review. *IOP Conference Series: Earth and Environmental Science*, 58, 012015. <https://doi.org/10.1088/1755-1315/58/1/012015>
- Tillman, G., Van Zandt, T., & Logan, G. D. (2020). Sequential sampling models without random between-trial variability: The racing diffusion model of speeded decision making. *Psychonomic Bulletin & Review*, 27(5), 911–936.
- Tukey, J. W. (1977). Exploratory data analysis.
- Tukey, J. W. (1979). Robust Techniques for the User. *Robustness in Statistics*, 103–106. Elsevier. <https://doi.org/10.1016/B978-0-12-438150-6.50013-3>
- Ulrich, R. & Miller, J. (1994). Effects of truncation on reaction time analysis. *Journal of Experimental Psychology: General*, 123(1), 34–80. <https://doi.org/10.1037/0096-3445.123.1.34>
- Usher, M. & McClelland, J. L. (2001). The time course of perceptual choice: The leaky, competing accumulator model. *Psychological Review*, 108(3), 550–592. <https://doi.org/10.1037/0033-295X.108.3.550>
- Von Krause, M., Radev, S. T., & Voss, A. (2022). Mental speed is high until age 60 as revealed by analysis of over a million participants. *Nature Human Behaviour*, 6(5), 700–708. <https://doi.org/10.1038/s41562-021-01282-7>
- Voss, A. & Voss, J. (2008). A fast numerical algorithm for the estimation of diffusion model parameters. *Journal of Mathematical Psychology*, 52(1), 1–9. <https://doi.org/10.1016/j.jmp.2007.09.005>
- Wabersich, D. & Vandekerckhove, J. (2014). Extending JAGS: A tutorial on adding custom distributions to JAGS (with a diffusion model example). *Behavior Research Methods*, 46(1), 15–28. <https://doi.org/10.3758/s13428-013-0369-3>
- Wagenmakers, E.-J., Van Der Maas, H. L. J., & Grasman, R. P. P. P. (2007). An EZ-diffusion model for response time and accuracy. *Psychonomic Bulletin & Review*, 14(1), 3–22. <https://doi.org/10.3758/BF03194023>
- Ward, D., Cannon, P., Beaumont, M., Fasiolo, M., & Schmon, S. M. (2022). *Robust Neural Posterior Estimation and Statistical Model Criticism*. <http://arxiv.org/abs/2210.06564>. arXiv:2210.06564 [cs, stat]

- Wieschen, E. M., Voss, A., & Radev, S. (2020). Jumping to Conclusion? A Lévy Flight Model of Decision Making. *The Quantitative Methods for Psychology*, 16(2), 120–132. <https://doi.org/10.20982/tqmp.16.2.p120>
- Wu, L. L. (1985). Robust m-estimation of location and regression. *Sociological Methodology*, 15, 316–388.
- Yang, L., Zhang, Z., Song, Y., Hong, S., Xu, R., Zhao, Y., Zhang, W., Cui, B., & Yang, M.-H. (2023). Diffusion models: A comprehensive survey of methods and applications. *ACM Computing Surveys*, 56(4), 1–39.
- Zaheer, M., Kottur, S., Ravanbakhsh, S., Poczos, B., Salakhutdinov, R. R., & Smola, A. J. (2017). Deep sets. *Advances in neural information processing systems*, 30.
- Zammit-Mangion, A., Sainsbury-Dale, M., & Huser, R. (2024). Neural methods for amortized inference. *Annual Review of Statistics and Its Application*, 12.

# Appendix

## Parameter Recovery Study for the Drift Diffusion Model

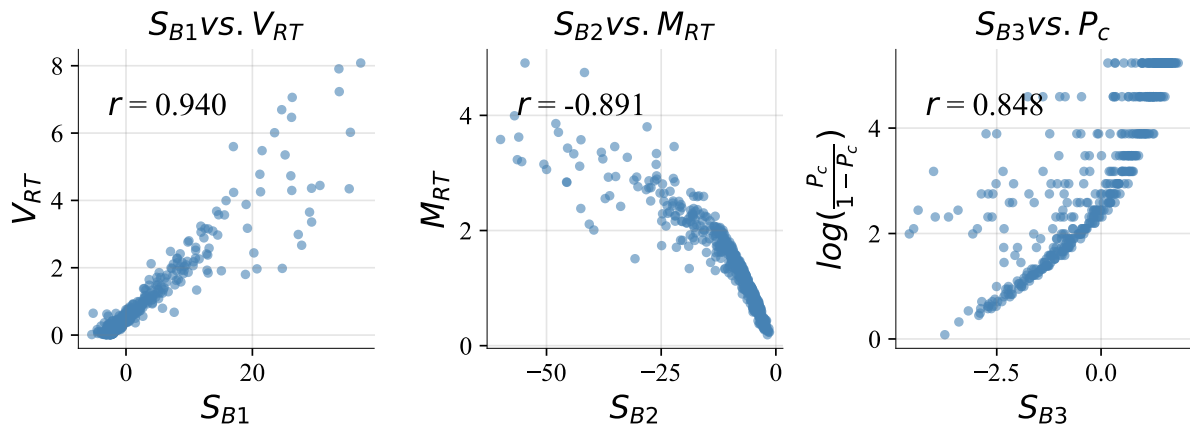


Figure A1: The non-linear relationship between  $\mathcal{S}_B$  and  $\mathcal{S}_{EZ}$ . Three summary statistics from EZ diffusion estimation are plotted against three summary statistics learned by BayesFlow, respectively.

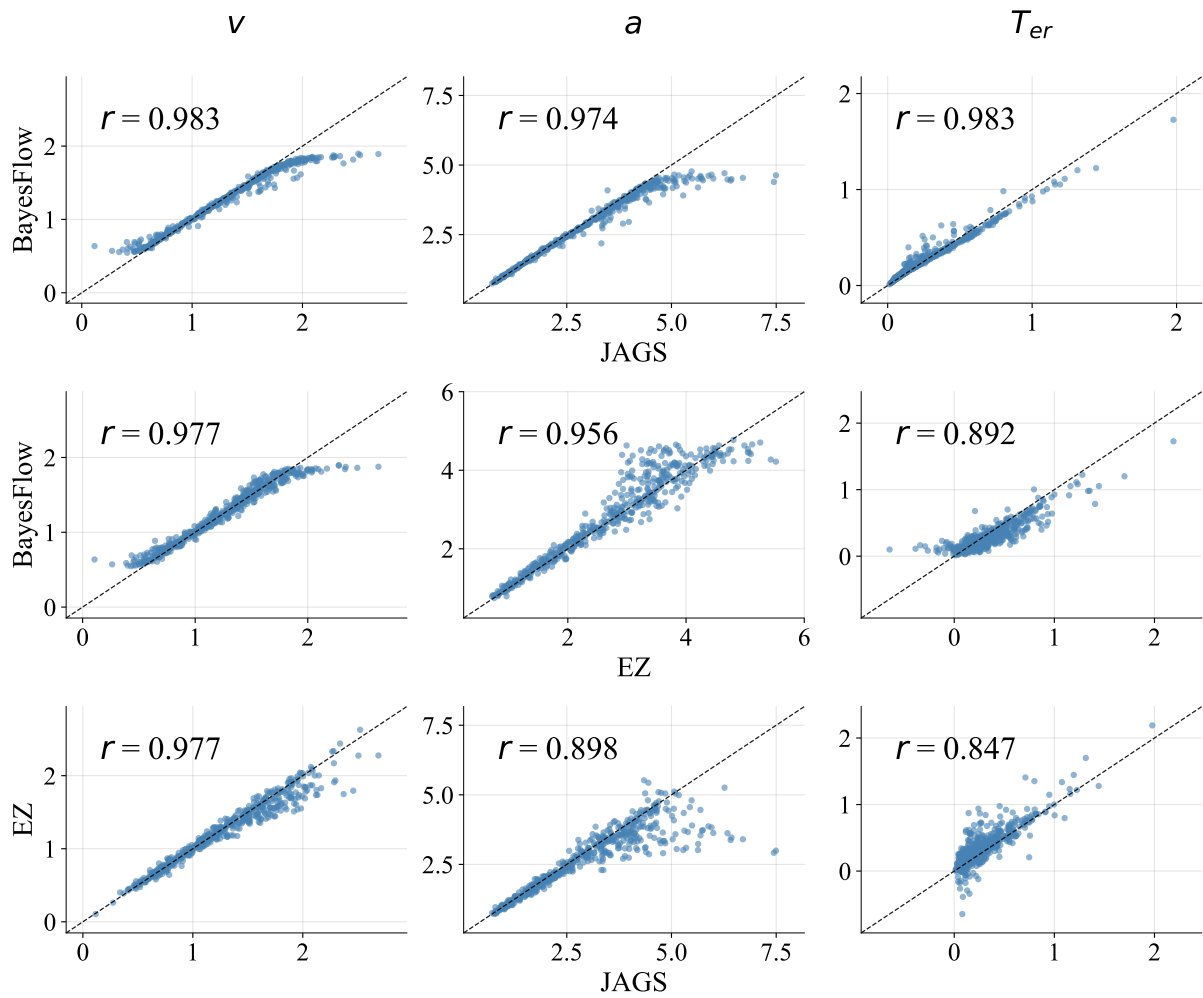


Figure A2: A comparison of different estimators. 500 data sets are simulated and fitted to JAGS, BayesFlow, and EZ diffusion. The first row shows the estimation of JAGS against that of BayesFlow, The second row shows the comparison between JAGS and EZ diffusion, and the third row is the relationship between EZ diffusion estimates and BayesFlow estimates.

## Robust Estimators with Different Contamination Probability $\pi$

Through the simulations presented in the mainbody of this paper, we found Cauchy distribution as contamination distribution optimal in training robust neural density estimator. We further explore the impact of contamination probability  $\pi$  when applying the Cauchy distribution in both the toy example and DDM. Specifically, we train robust neural estimators with  $\pi \in \{0.01, 0.05, 0.10, 0.20\}$ , respectively. Robust estimators in the mainbody have  $\pi = 0.10$ .

The network architectures are identical for all the  $\mu$  estimators as specified in the mainbody text, with 10 epochs, 4000 iterations per epoch, and a batch size of 32. Afterwards, we investigate the robustness of  $\mu$  estimators with EIF and BP. As the Figure A3 shows, the EIFs show similar shape for all the robust estimators, while the BP plot reveals that the estimator with  $\pi = 0.01$  has a lower BP, thus lower level of robustness. Table A1 shows us the error ratio and variance ratio of robust estimators decreases with the increase of  $\pi$ , indicating that the accuracy and efficiency losses are lower for less robust estimators.

The network architectures and training setting are the same for all the DDM estimators through out the whole paper. We investigate the EIF and BP of four robust DDM estimators, and found that the higher the  $\pi$ , the less empirical influence an outlier has on estimation, especially when there is a short outlier (see Figure A4a and A4b). In terms of BP, the estimators with  $\pi = 0.10$  and  $0.20$  show a higher BP than the other two estimator to short outliers ( $rt^c = 0.01s$ ), while the estimators with  $\pi = 0.05$  and  $0.10$  show a higher BP to long outliers ( $rt^c = 20s$ ). The robustness and efficiency losses trade-off appears again in the variance ratio of robust DDM estimators and standard DDM estimators: the higher the  $\pi$ , the smaller the variance ratio, thus larger efficiency losses.

To summarize, varying  $\pi$  does have an effect on the performance of robust estimators. While  $\pi = 0.01$  can be too low in terms of robustness,  $\pi = 0.20$  is too high in terms of efficiency loss, a  $\pi$  from  $0.05$  and  $0.10$  allow us to balance these two properties, thus are more suitable to be used in practice.

Robust estimator	MAE Ratio	Posterior Variance Ratio
$\pi = 0.01$	1.003	0.981
$\pi = 0.05$	1.000	0.945
$\pi = 0.10$	0.996	0.913
$\pi = 0.20$	0.978	0.863

Table A1: MAE ratio and posterior variance ratio of location parameter estimators with different contamination probabilities  $\pi$ . This table shows MAE ratio and posterior variance ratio between a standard estimator and the robust estimator. In each row, the robust estimator has a  $t_1$  as the contamination distribution and contamination probability  $\pi$ .

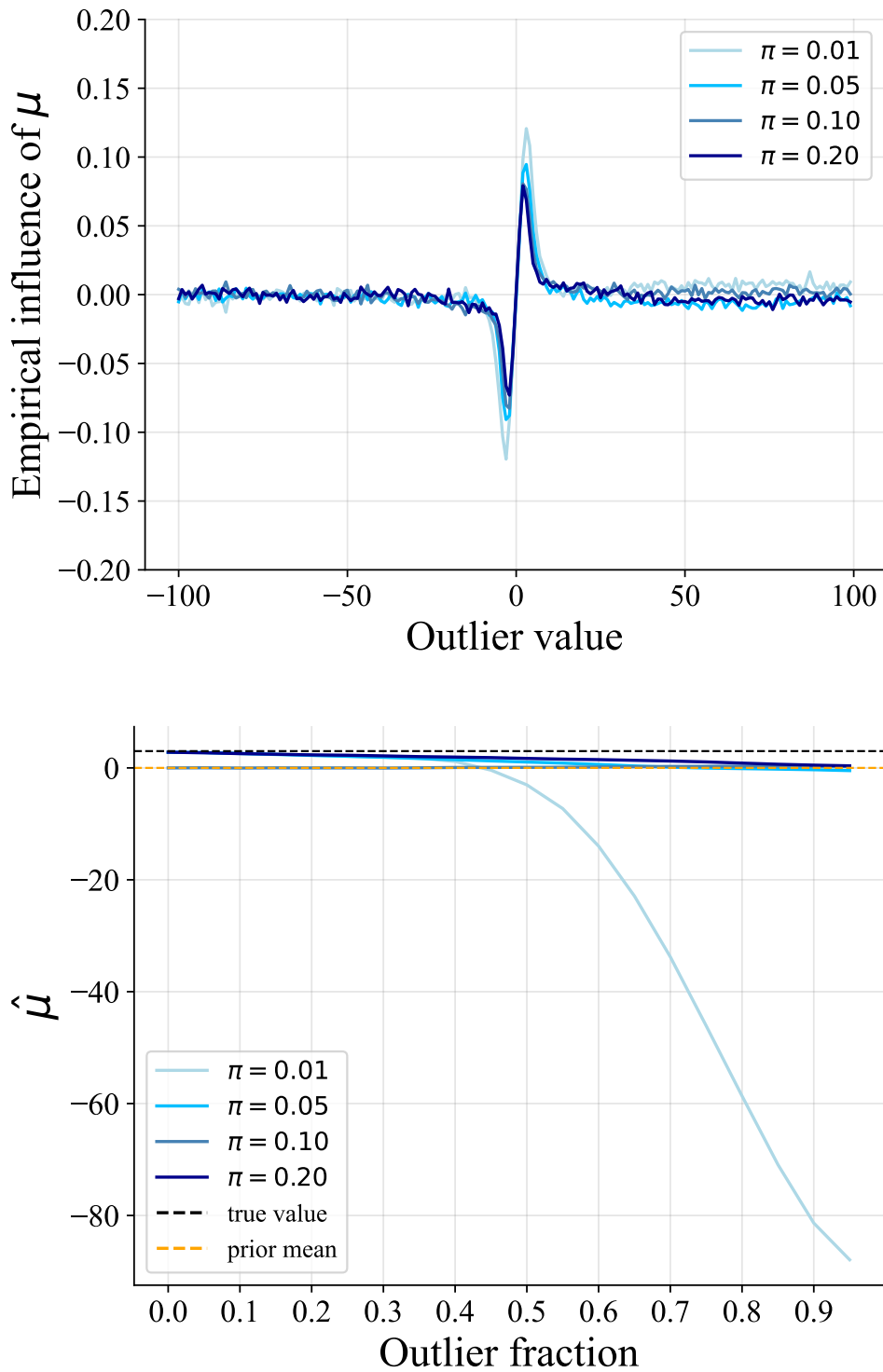
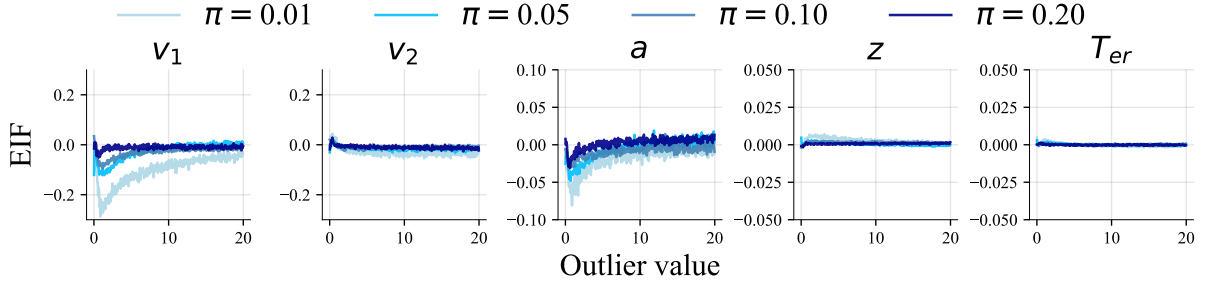
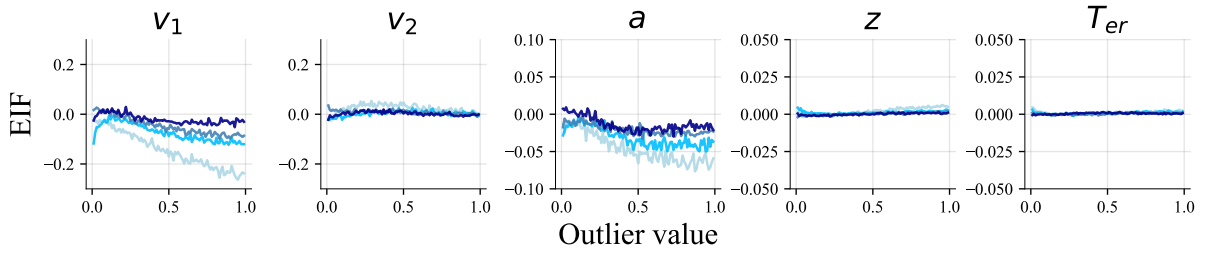


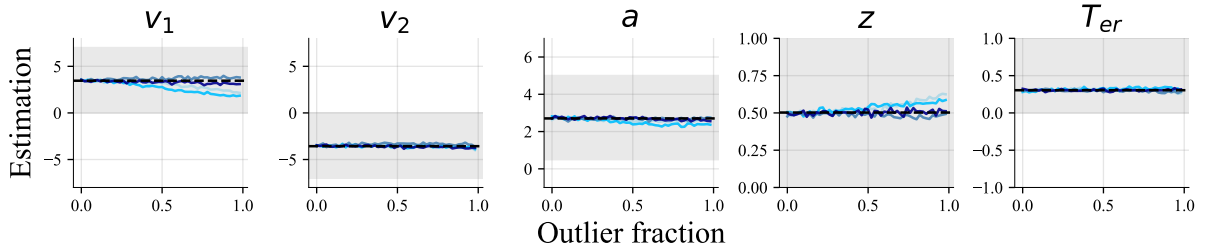
Figure A3: The normal robust estimators with contamination distribution  $t_1$  and different contamination probability  $\pi$ . The upper plot shows the EIF of the robust estimators with outliers ranging from -100 to 100 (increasing by 1). The lower plot shows the breakdown point with outlier values fixed at -100.



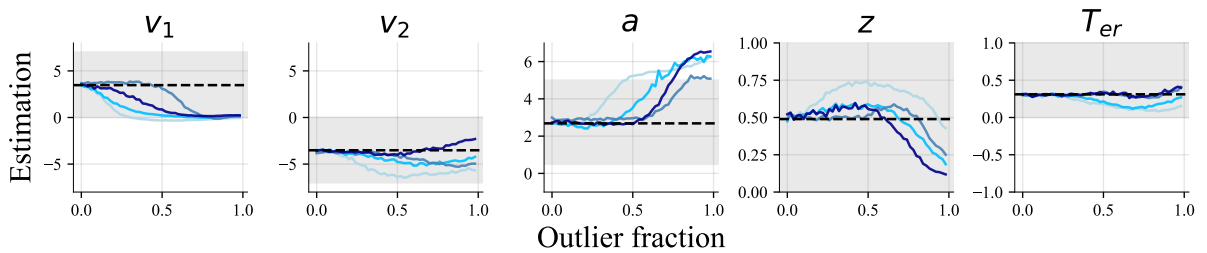
(a) EIF for DDM parameter in robust estimators with  $rt^c$  from 0.01 to 20s.



(b) EIF for DDM parameter in robust estimators with  $rt^c$  from 0.01 to 1s



(c) BP for DDM parameters in robust estimators with  $rt^c = 0.01s$  and contamination fraction  $p$



(d) BP for DDM parameters in robust estimators with  $rt^c = 20s$  and contamination fraction  $p$

Figure A4: The DDM robust estimators with contamination distribution folded- $t_1$  and different contamination probability  $\pi$ . Row (a) shows the EIF of the robust estimators with outliers ranging from 0.01s to 20s (increasing by 0.05s). Row (b) shows the EIF with outliers ranging from 0.01s to 1s (increasing by 0.01s). Rows (c) and (d) display the breakdown point plots with outlier values fixed at 0.01s and 20s, respectively.



Robust estimator	$v_1$	$v_2$	$a$	$z$	$T_{er}$
$\pi = 0.01$	0.759	0.802	0.777	0.907	0.826
$\pi = 0.05$	0.73	0.732	0.735	0.892	0.797
$\pi = 0.10$	0.728	0.751	0.741	0.889	0.764
$\pi = 0.20$	0.875	0.907	0.916	0.965	0.884

Table A2: MAE ratio in DDM estimators with different  $\pi$ . This table shows the MAE ratio between a standard estimator and a robust estimator. In each row, the robust estimator has a folded- $t_1$  as the contamination distribution and a certain contamination probability  $p_i$ .

Robust estimator	$v_1$	$v_2$	$a$	$z$	$T_{er}$
$\pi = 0.01$	0.823	0.807	0.885	0.978	0.864
$\pi = 0.05$	0.720	0.699	0.74	0.819	0.71
$\pi = 0.10$	0.617	0.596	0.615	0.734	0.574
$\pi = 0.20$	0.436	0.517	0.531	0.574	0.492

Table A3: Posterior variance ratio of DDM estimators with different  $\pi$ . This table shows the posterior variance ratio in estimates between a standard estimator and a robust estimator. In each row, the robust estimator has a folded- $t_1$  as the contamination distribution and a certain contamination probability  $\pi$ .